Statistical Characteristics of Mesoscale Fluctuations of Wind Velocity, Temperature, and Gas Concentrations Obtained from Aircraft Measurements in the Troposphere of the Arctic Region

I. CHUNCHUZOV,[a] O. CHKHETIANI,[a] S. KULICHKOV,[a] O. POPOV,[a] B. BELAN,[b] A. FOFONOV,[b] G. IVLEV,[b] AND A. KOZLOV[b]

[a] *Obukhov Institute of Atmospheric Physics, Moscow, Russia*
[b] *V. E. Zuev Institute of Atmospheric Optics, Tomsk, Russia*

(Manuscript received 17 February 2023, in final form 20 September 2023, accepted 3 October 2023)

ABSTRACT: The results of airborne measurements and statistical characteristics of mesoscale fluctuations of wind velocity, temperature, and concentrations of gas constituents at different heights of a stably stratified troposphere are presented. The measurements were carried out in September 2022 in the Arctic region of Russia with the aircraft laboratory Tu-134 "Optik." The obtained spectra and structure functions of the fluctuations are interpreted with the theoretical model of formation of the spectrum of mesoscale wind velocity and temperature fluctuations described in the paper. The presence at high wavenumbers of a steep section in the obtained horizontal wavenumber spectra of the fluctuations of wind velocity and greenhouse gas concentration with a slope close to −3 is discussed. The fluctuation spectra along different slanted tracks of the aircraft crossing the tropospheric layer between altitudes of 1 and 9 km are also obtained and analyzed with the theoretical model.

KEYWORDS: Advection; Internal waves; Turbulence; Troposphere; Atmospheric waves

1. Introduction

The studies of the aircraft measured fluctuations of meteorological parameters (wind velocity components, temperature, pressure, humidity) and concentrations of gas components in the troposphere and lower stratosphere, carried out during the last few decades, significantly contributed to our understanding of the statistical characteristics of these fluctuations (variances, spectra, structure functions) in a wide range of their horizontal scales (Lilly and Lester 1974; Vinnichenko et al. 1980; Nastrom and Gage 1985; Bacmeister et al. 1996; Cho et al. 1999; Hertzog et al. 2002; Gurvich and Kukharets 2008; Waite and Snyder 2014; Callies et al. 2014, 2016; Lindborg 2015; Zhang et al. 2015; Craig and Selz 2018; Schumann 2019; Stephens et al. 2021; Dörnbrack et al. 2022; Imazio et al. 2023). These measurements revealed the presence in the atmosphere of both the internal gravity waves (IGWs) with nonzero horizontal divergence and horizontal vortical motions with the zero horizontal divergence (Callies et al. 2014, 2016; Lindborg 2015; Schumann 2019). The explanation of the mechanism of formation of the energy spectrum of the atmospheric fluctuations induced by IGWs and vortical motions, and parameterization of their statistical characteristics, are necessary for modeling the processes of pollution transport and long-range propagation of sound and light in the atmosphere.

The question on the relative contributions of IGWs and horizontal vortical motions to the formation of the horizontal wavenumber spectrum of mesoscale wind velocity and temperature fluctuations in the upper troposphere and lower stratosphere is still debated (Waite and Snyder 2014; Callies et al. 2014; Skamarock et al. 2014; Lindborg 2015). The combination of airborne measurement methods and modeling of wind and temperature field variations using a high-resolution numerical weather forecast model allowed Dörnbrack et al. (2022) to detect and analyze the case of internal gravity wave generation by a propagating Rossby wave train.

The mechanism of formation in a stably stratified atmosphere of the −5/3 spectrum in the range of horizontal scales from about 500 km to several kilometers has been discussed since the end of the last century (Gisina 1969; Lilly and Lester 1974; Gage 1979; Dewan and Good 1986; Dewan 1997; Lindborg 1999; Cho et al. 1999) and up to the present (Golitsyn 2012; Waite and Snyder 2014; Callies et al. 2014; Lindborg 2015; Skamarock et al. 2014; Žagar et al. 2017; Poblet et al. 2022). In this scale range the spectrum obtained from the aircraft measurements by Nastrom and Gage (1985) decreases with increasing horizontal wavenumber according to the −5/3 law.

Analyzing the spectral balance equations of turbulence energy in a thermally stratified medium, Gisina (1969) showed that in a stably stratified atmosphere there may be a "−5/3 law" in the region of wavenumbers, which are significantly affected by buoyancy. However, this law differs significantly from the Kolmogorov–Obukhov law because the spectral characteristics do not depend on the mean turbulence energy dissipation rate. In the wavenumber region under consideration, the generation by the average wind shear of the energy of turbulence is compensated by the work of turbulence against buoyancy forces (energy dissipation and energy transfer along the spectrum in this region can be neglected). Later, two opposing hypotheses were suggested to explain the mechanism of formation of the $k^{-5/3}$ horizontal wavenumber spectrum. It has been suggested that such a spectrum can result either from an inverse energy cascade from small horizontal

Corresponding author: Igor Chunchuzov, igor.chunchuzov@gmail.com

DOI: 10.1175/JAS-D-23-0021.1

scales to larger scales, similar to that observed in two-dimensional turbulence (Gage 1979), or from a direct cascade energy transfer from large-scale internal waves to small-scale wave disturbances (Dewan and Good 1986; Dewan 1997).

Lindborg (2006) also suggested the existence of a downscale turbulence energy cascade in the mesoscale range, arising in the presence of strong stable stratification of the medium, i.e., in the limit of small horizontal Froude number $F_h = \varepsilon^{1/3}/(Nl_h^{2/3})$, where ε is the mean energy dissipation rate of mesoscale motions, l_h is their horizontal scale, and N is the Brunt–Väisälä frequency. In the presence of strong stable stratification the 2D vertically oriented vortices with a horizontal length scale l_h will divide into layers with a vertical length scale $l_v \sim F_h l_h$. These layers divide into thinner layers, which, in turn, divide into even thinner layers, and so on. From similarity and dimensionality theory the following expressions were obtained for the spectra of kinetic and potential energies of mesoscale motions: $E_k(k_x) = C_K \varepsilon_K^{2/3} k_x^{-5/3}$, $E_P(k_x) = C_P \varepsilon_K^{-1/3} \varepsilon_P k_x^{-5/3}$, where ε_K is the mean dissipation rate of kinetic energy, ε_P is the mean dissipation rate of potential energy, and C_P and C_K are the numerical constants of order 0.5, as followed from numerical simulations of the thin-layer formation process.

It should be noted that before the work of Lindborg (2006), the process of thin layers emergence in the stably stratified medium was predicted in the works of Chunchuzov (1996, 2002). In these and subsequent works (Chunchuzov 2009, 2018) it was shown that nonlinear nonresonant interactions of internal waves generated by their random sources (wind shear instability, meteorological fronts, solar terminator, convection, orography, jet streams) at some vertical and horizontal scales transfer wave energy toward shorter vertical scales and, simultaneously, longer horizontal scales. Due to such an energy transfer the layered inhomogeneities of temperature and wind velocity are formed with strongly anisotropic 3D spectrum in the region of high vertical wavenumbers. This spectrum is independent of random spectrum of the wave sources themselves specified in the Lagrangian variables. At the same time, the corresponding 1D (horizontal and vertical) wavenumber spectra decay with increasing wavenumbers according to the -3 power law at certain scale ranges.

It is important to note that earlier studies of the horizontal wavenumber spectra of wind velocity and temperature fluctuations obtained from aircraft measurements under stable stratification of the troposphere and lower stratosphere (Shur 1962; Myrup 1969; Lilly and Lester 1974; Vinnichenko et al. 1980; Bacmeister et al. 1996) pointed to the presence of a transition from the $-5/3$ (or -2) law to a steeper spectrum in the range of scales from about 6 km to 300 m. Above the mountainous terrain, the transition mentioned above occurred in the stratosphere and the upper troposphere at longer horizontal scales of 15–23 km (Nastrom et al. 1987). It is the presence of such a steep horizontal wavenumber spectrum of mesoscale fluctuations that was not taken into account in the most of modern models of its formation, but was predicted in the earlier studies mentioned above and theoretical model developed in Chunchuzov et al. (2018).

A distinctive feature of the early aircraft measurements of wind velocity and temperature fluctuations at different altitudes of the troposphere and lower stratosphere was the study of the influence of temperature stratification (neutral, convectively unstable, and stable) on the forms and slopes of spectra in different horizontal scale ranges (Myrup 1969; Vinnichenko et al. 1980). These measurements were accompanied by frequent radiosonde and balloon measurements of the temperature and wind vertical profiles in order to follow the changes in the slopes of individual horizontal spectra of wind velocity and temperature fluctuations caused by changes in the stratification of the troposphere. In Fig. 1 of Myrup (1969) the temperature profiles for different time periods were shown for different time periods of the flight. In Vinnichenko et al. (1980) the radiosonde data were also used to analyze thermal stratification at different altitudes of the flight segments, but temperature profiles were not shown

Under the neutral stratification of the lower troposphere the measurements of the horizontal wind velocity fluctuations along the aircraft route at an altitude of 3 km resulted in individual fluctuation spectra with a slope close to $-5/3$ in the range of horizontal scales from 20 km to 400 m (see Fig. 4.5a in Vinnichenko et al. 1980). Above an altitude of 6 km the thermal stratification of the troposphere was stable, and an increase in the slopes of individual spectra at 9-km height in the range of scales from about 6 km to 400 m was observed, compared to the slope of the $-5/3$ spectrum at larger scales (greater than 6 km), and to the slope of $-5/3$ Kolmogorov–Obukhov spectrum at shorter scales, below 400 m (see Fig. 4.5d in Vinnichenko et al. 1980).

The dependence of the spectral forms on the thermal stratification of the lower troposphere was also clearly manifested in the Myrup (1969) experiment, where the horizontal and vertical wind velocity fluctuations were measured over a dried lake in the desert of Northern California (United States). In the early morning hours (about 0600 LT), a stable stratification was observed in the lower troposphere with a strong inversion over the dried lake to a height of about 600 m. After sunrise an intense convection changed the stratification of the lower troposphere from stable to neutral one. The energy spectra of the horizontal wind velocity fluctuations measured at 0655 local time at a height of 300 m, and at 0910 LT, showed that under stable stratification in the early morning the slope of spectral curve was close to -3, whereas under neutral stratification the slope was practically coincided with a $-5/3$ slope. As to the spectra of the vertical wind velocity component, measured at around 0700 and 0850 LT the slope in the frequency range < 1 Hz (the horizontal scales more than 69 m for the airborne mean speed of 69 m s^{-1} at a height of 300 m) was between -3 and $-11/5$ under stable stratification, and was close to $-5/3$ under neutral stratification (Myrup 1969). According to radiosonde data the rearrangement of the tropospheric stratification from stable to neutral one at flight level occurred between 0800 and 0830 LT.

It is due to the control of stratification of the troposphere in the experiments of Myrup (1969) and Vinnichenko et al. (1980) that the transition from a $-5/3$ spectrum at neutral stratification to a steeper one (with slopes from -2.5 to -3 at

horizontal scales from 6 km to 400 m) under stable stratification of the troposphere was found.

Cho et al. (1999), discussing the presence of a transition in the spectra obtained by Bacmeister et al. (1996) on some scale of about 3 km to a steeper spectrum, noted "our full spectral results for horizontal velocity and potential temperature, which covered a range of about 0.5–100 km, did not display such break points, even at altitudes above 11 km." Nevertheless, Cho et al. note, referring to the results of airplane measurements by Nastrom et al. (1987) in the mountainous region, that a subset of GASP spectra did have such a break point (at wave lengths of ~15 km in the stratosphere and ~23 km in the troposphere), over mountainous terrain in high wind conditions. They conclude, "If a departure from a −5/3 slope was due to extra energy injected by orographically generated gravity waves, then the lack of a break point in our spectra is consistent with the fact that the PEM flights were conducted over the ocean…" This conclusion of Cho et al. (1999) confirms the connection noted above between the presence of the transition to the steep spectrum and the stable stratification of the troposphere under which orographic gravity waves can propagate.

In more recent experiments the airborne measurements have been performed on long traces with a large number of segments (Callies et al. 2014, 2016; Skamarock et al. 2014; Lindborg 2015; Li and Lindborg 2018). In these works, the data on stratification and stability of tropospheric layers through which the flights passed were not given, so we assumed that long segments of 1000 km or more passed through regions of the troposphere with different stratification, including areas of small-scale turbulence with neutral stratification, and areas with stable stratification. The averaging spectra with different slopes (from −5/3 to −3) over a large number of segments should result in an average spectrum with some intermediate slope lying between −5/3 and −3. In the recent experiments mentioned above the horizontal spectra obtained were close to −5/3, whereas in the earlier experiments of Myrup (1969), Vinnichenko et al. (1980), Bacmeister et al. (1996), and in our measurements in the Arctic region (see below) with mostly stable stratification in the troposphere the slopes of the spectra were between −2.5 and −3 at short scales, between 400 m and 6 km.

By applying a wave–vortex decomposition method to two datasets collected aboard commercial and research aircrafts Callies et al. (2016) showed that the relative magnitudes of mesoscale fluctuations of along-track velocity, across-track velocity, and buoyancy with the horizontal scales from 100 to 10 km are consistent with the dispersion and polarization relations of inertia–gravity waves. They found that the observed spectra become steeper at scales smaller than 10 km, which "contradicts the alternative explanation of mesoscale variability using the theory of stratified turbulence." As shown by Chunchuzov (2018) the observed steepening of the horizontal spectrum at scales of less than 10 km is due to the fact that these scales become comparable with the horizontal displacements of the air parcels caused by all internal gravity waves, including the inertia–gravity waves, so that the nonlinear interactions between these waves become strong.

Using 3 years of analysis data from a kilometer-scale numerical weather prediction system Craig and Selz (2018), and Selz et al. (2019) investigated the variability of the mesoscale kinetic energy (KE) spectrum in slope and amplitude, and the dynamical processes that affect this variability. They found that mesoscale KE spectrum varies systematically with environmental factors; therefore, their study "does not support the hypothesis of a universal mesoscale KE spectrum…" Particularly, a high variability of the spectral amplitudes and slopes at horizontal scales less than 100 km was found to be correlated with high convection and precipitation rates. The exceptionally steep slope of −3.14 was found for the KE spectrum in the entire range of scales from 1000 to 10 km (see Fig. 6 in Selz et al. 2019), when the KE is enhanced at large scales (500–1000 km) due to a strong potential vorticity anomaly and reduced at smaller scales (100–10 km) due to an almost complete absence of convection and precipitation. Another extreme case of a shallow KE spectrum with a slope of −1.74 was associated with enhanced convective activity and precipitation at scales less than 100 km. The cases considered by Selz et al. (2019) of an increase in the slope of the KE spectrum due to the transition from strong convection to its complete absence were also accompanied by a transition from unstable to stable stratification of the atmosphere.

Li and Lindborg (2018) calculated horizontal temperature and kinetic energy (rotational and divergent) spectra from the Measurement of Ozone and Water Vapor by Airbus In-Service Aircraft (MOZAIC) dataset. The spectra were obtained up to minimum (cutoff) horizontal scale of 4 km. They observed the extending of the $k^{-5/3}$ range to the cutoff wavelength $l = 4$ km in the upper troposphere, and up to $l = 10$ km in the lower stratosphere. In the stratosphere they found a transition from $k^{-5/3}$ spectrum to a steeper spectrum; however, they did not find such transition in the upper troposphere. A similar transition as noted by Li and Lindborg (2018) was observed by Bacmeister et al. (1996) and Callies et al. (2016), when they used the START08 data. When these authors analyzed MOZAIC data they used a larger cutoff wavelength, of order 20 km, as compared to 4 km used by Li and Lindborg (2018), and could therefore not detect this transition.

Vinnichenko et al. (1980) also observed under stable stratification of the troposphere at 9-km height an increase in the slopes of temperature spectra in the range of scales from about 6 km to 400 m compared to the slope of the −5/3 spectrum at scales greater than 6 km. In the spectra obtained by Li and Lindborg (2018) the most part of the transitional interval from 6 km to 400 m was laying lower than the cutoff length scale $l = 4$ km; therefore, a transition to the steeper spectrum could not be observed. Besides this, no sounding data were presented in this paper indicating that the stratification in the tropospheric layer containing the most part of the flight segment was stable. It is in the conditions of stable stratification of the tropospheric layer that the transition from the −5/3 spectrum to a steeper spectrum could be observed. The stratosphere is normally about twice as stable as the troposphere (in terms of its Brunt–Väisälä frequency N) (Lane 2015; Nappo 2012). In the lower stratosphere Li and Lindborg (2018) did observe a transition to a steeper spectrum at scales

less than 10 km. The increase of the characteristic horizontal scale in the stratosphere compared to the troposphere, at which such a transition takes place, can be explained by an increase with height of the rms wind velocity fluctuations due to a decrease of mean atmospheric density (Chunchuzov 2018).

Recently, Imazio et al. (2023) carried out measurements of the three wind velocity components, when the aircraft flew through separate "patches" of turbulence in the troposphere over the southern Andes. Although Imazio et al. (2023) had no access to measurements of stratification they relied on NWP data (from the IFS of ECMWF) which they interpolated on their aircraft trajectories. A possible source of the "patches" of turbulence could be instabilities of mountain waves propagating into the upper troposphere. For some "patches," the horizontal spectra of velocity fluctuations for the scales from 1 km to 50 m followed a power law close to −5/3. For other "patches" the spectra with slopes from −1.9 to −2.5 were observed, which the authors attributed to the anisotropy of the turbulent airflow. These measurements confirm the existence of the intermittency of mesoscale turbulence and sensitivity of the slopes of the observed horizontal spectra of wind fluctuations to the changes of the atmospheric stratification along flight segments. Earlier, the same conclusion also followed from aircraft measurements in the lower troposphere under the control of its temperature and wind stratification (Myrup 1969; Vinnichenko et al. 1980). Under convection or neutral stratification in the lower troposphere, the slopes of the measured horizontal spectra were close to −5/3, whereas under stable stratification of the tropospheric layers the spectral slopes were close to −3.

The present work is devoted to studying the statistical characteristics (spectra and structure functions) of mesoscale fluctuations of wind velocity, temperature, and gas concentrations at different altitudes of the stably stratified troposphere obtained from the Tu-134 "Optik" laboratory aircraft measurements carried out in September 2022 in the Arctic region of Russia. The model of formation of mesoscale fluctuations spectra will be presented in section 2. The description of the measuring routes of the aircraft, meteorological conditions, and stratification of the troposphere will be given in section 3. The analysis and theoretical interpretation of the horizontal and slanted spectra of fluctuations obtained in conditions of stable stratification of the troposphere will be given in sections 4 and 5.

2. Formation model for the spectrum of anisotropic fluctuations in a stably stratified atmosphere

In the works of Shur (1962), Myrup (1969), Lilly and Lester (1974), Vinnichenko et al. (1980), and Bacmeister et al. (1996) the horizontal fluctuation spectrum with a slope close to −3 was observed in the stably stratified layers of the troposphere at large scales compared to the scales of turbulence within its inertial range. The appearance of a steep part of the spectrum compared to the −5/3 Kolmogorov–Obukhov law was explained in the models of Shur (1962) and Lumley (1964) and Lumley and Panofsky (1964) by the fact that part of the kinetic energy of turbulent motions during its cascade transfer from large to small scales is converted into potential energy due to the work performed by turbulence against buoyancy forces in the stably stratified atmosphere. This theory as noted by Lumley is applicable in the buoyancy subrange whether the random velocity and temperature fluctuations in the stratified medium are caused by internal wave perturbations or by turbulent vortex motions.

By considering resonant and nonresonant interactions of internal waves in a stably stratified fluid caused by nonlinearity of their motion equations Phillips (1967) showed that nonresonant wave–wave interactions at large wavenumbers k cause cascading energy transfer from one wave mode to another, which leads to an equilibrium wave energy spectrum $E(k) \sim N^2/k^3$ decreasing according to the −3 law, where N is the buoyancy frequency. The spectrum he obtained from the assumption of a cascade caused by nonresonant wave–wave interactions coincides with the spectrum of turbulent fluctuations in a stably stratified medium obtained by Shur (1962) and Lumley (1964). Thus, the cascade-like energy transfer caused by strong nonresonant interactions of wave perturbations with a small interaction time and the turbulent cascade in a stably stratified medium result in the same spectrum in the buoyancy subrange with a slope of −3.

Note that in the spectrum models considered above the statistical homogeneity and isotropy of the fluctuations was implied. Assuming that random Lagrangian displacements and velocities of particles of stably stratified medium are caused by an ensemble of internal waves with randomly independent amplitudes and phases, are statistically homogeneous in some finite volume of medium and axially isotropic in horizontal plane, the spatial displacement and velocity spectra (3D, vertical and horizontal) were obtained by Chunchuzov (2001, 2002). The important conclusion of this theory was that at large wavenumbers the 3D spectra have a universal anisotropic form, independent of the form of the spatial spectrum of Lagrangian random sources of internal waves. The obtained spectra do not change in the case when the interactions of internal waves with vortical modes are also taken into account (Chunchuzov 2018).

To take into account the influence of stable stratification of the atmosphere and advection of air particles [described by the nonlinear term $(\mathbf{v}\nabla)\mathbf{v}$ in the equations of motion] on the wave spectrum formation, the Lagrangian approach was applied in Chunchuzov (1996, 2001, 2002, 2009), Eckermann (1999), and Hines (2001). Its essence was in that first the approximate solutions of the Lagrangian equations of motion for internal waves were found, taking into account their nonlinearity, and then the exact transformation from the Lagrangian to the Eulerian coordinates was performed (Chunchuzov 2009). This approach allowed us to take into account the influence on the wave spectrum of advection of internal waves in the wind velocity field created by the total field of all waves.

The 3D spectrum of the vertical displacements in the Eulerian coordinates obtained in the limiting case of high wavenumbers as shown in Chunchuzov (2018) does not depend on the spectrum of Lagrangian displacements caused by internal waves and vortical motions. Also, it does not provide any information on energy fluxes. This spectrum depends only on

the variances of the fluctuations of the horizontal gradients of the displacement components that can be expressed only through two parameters: the nonlinearity parameter of the wave field, $M \equiv \nu_V/l_v$, or Froude number $M \equiv \sigma/(Nl_v) \ll 1$, where ν_V and σ are rms values of the vertical displacements and wind velocity fluctuations, respectively, N is the Brunt–Väisälä frequency, l_v is the characteristic vertical scale of random sources of waves and vortices, and the parameter $\chi = \nu_1/\nu_V = \sigma/\sigma_V \gg 1$ characterizes the anisotropy of the Lagrangian displacement or velocity fields, where σ_v is the rms value of the Lagrangian fluctuations of vertical velocities. In the wavenumber space, the resulting 3D spectrum is localized at high vertical wavenumbers $|k_z| \gg m^*$ (i.e., short vertical scales), and small horizontal wavenumbers, $k_\perp \leq 2\sqrt{e_0}k_z$, where

$$m^* = 1/\left(\nu_V\sqrt{2}\right) = N/(\sqrt{2}\sigma) \tag{1}$$

is the characteristic vertical wavenumber, and $e_0 \sim M^2/\chi^2 \ll 1$ is the dimensionless parameter that characterizes the anisotropy of emerging layered inhomogeneities in the wind and temperature fields, corresponding to the surfaces of a constant spectral amplitudes in the wavenumber space.

a. Vertical wavenumber spectra of the displacements and velocities

The advection of internal waves by the varying in space and time wind caused by internal waves and vortices leads to generation of the spectral "tail" at large vertical wavenumbers k_z with the following forms for vertical displacements

$$S_{1E}(k_z) = \beta k_z^{-3}, \quad m^* \ll k_z < m_c \tag{2}$$

and horizontal velocities (Chunchuzov 2018):

$$V_E(k_z) = \alpha N_1^2 k_z^{-3}, \quad m^* \ll k_z < m_c, \tag{3}$$

where the dimensionless coefficients β and α increase from zero along with the nonlinearity parameter M, reaching maximum values of 0.1–0.2 at $M \sim 0.3$, at which the spectrum becomes nonlinearly saturated, and $N = N_1 = \text{const}$ is the buoyancy frequency in the chosen stably stratified atmospheric layer. Knowing the spectrum of vertical displacements (2), we can multiply it by N^4/g^2, where g is the acceleration of gravity, and obtain the spectrum of relative temperature fluctuations. As a result, using (2) and (3) the spectrum of temperature fluctuations can be expressed as follows:

$$S_T(k_z) = T_0^2 \times (N^4/g^2)S_{1E}(k_z) = T_0^2 \times (N^2/g^2)V_E(k_z), \tag{3a}$$

where T_0 is the average temperature.

The resulting spectra (2)–(3a) decrease along with the vertical scale of the fluctuations according to the −3 power law. The k_z^{-3} spectrum is bounded from below by a characteristic vertical wavenumber $m^* \sim N/\sigma$ at which the horizontal phase speeds of the internal waves N/k_z become comparable to the rms wind velocity fluctuations σ caused by the waves themselves. From above, the k_z^{-3} spectrum is bounded by the critical wavenumber $m_c = m^* \exp(1/\beta)$, where $\beta \approx 0.2$ under nonlinear saturation of the spectrum, at which in some local regions of space there arise breaking processes of internal waves due to wave-induced convective or shear instabilities. The wave breaking processes lead to the generation of thin layers of small-scale turbulence with vertical scales of vortices less than $2\pi m_c^{-1}$. The resulting thin turbulence layers at different heights intermittent with stably stratified layers whose vertical scales are greater than $2\pi m_c^{-1}$.

In case of passive tracers the fluctuations of their concentration q at a certain height z are caused mainly by vertical displacements of air particles in a presence of the average gradient of gas concentration dq_0/dz, so the vertical wavenumber spectrum of fluctuations q can be expressed through the displacement spectrum (2) or wind velocity spectrum (3):

$$S_q(k_z) = (dq_0/dz)^2 S_{1E}(k_z) = (dq_0/dz)^2 N^{-2} V_E(k_z). \tag{3b}$$

b. Horizontal spectra

The horizontal wavenumber spectrum of wind velocity fluctuations was shown to decrease as k_x^{-3} at large horizontal wavenumbers k_x (Chunchuzov 2018):

$$\tilde{V}_{E,\perp}(k_x) = 4e_0\alpha_0 N^2 k_x^{-3}, \quad k_x \gg k^* = 2\sqrt{e_0}m^*, \tag{4}$$

where k^* is the characteristic horizontal wavenumber. Its ratio to the vertical wavenumber $m^* = 1/(\sqrt{2}\nu_V) = N/(\sqrt{2}\sigma)$ determines the anisotropy coefficient $2e_0^{1/2} \ll 1$ of layered wind velocity inhomogeneities, and the amplitude of the horizontal spectrum (4) is $(4e_0)^{-1}$ times lower than that of the vertical spectrum (3). Thus, in the interval of short vertical scales, $2\pi/m_c < l_z < 2\pi/m^*$, there exist similar in shape anisotropic wind velocity inhomogeneities with the same ratio of scales $l_x/l_z = 1/\sqrt{4e_0} \gg 1$. Their outer vertical scale is $L_v^* = 2\pi/m^*$, whereas the corresponding horizontal scale at which the transition to the steep spectrum (4) takes place is $L_\perp^* = 2\pi/k^*$, which, according to (1) and (4), is proportional to the rms value of wind velocity fluctuations, and inversely proportional to buoyancy frequency N and the anisotropy coefficient $2e_0^{1/2} \ll 1$. Below we use the theoretical model of mesoscale wind velocity fluctuation spectrum formation briefly outlined here to interpret the obtained spectra from airplane measurement data.

3. Aircraft measurement routes and meteorological conditions in the Arctic region in September 2022

The 3D graph of the aircraft flight path in coordinates of latitude, longitude, and altitude, and almost horizontal sections of the aircraft flights (segments 1 and 2), along which the measurements of flight altitude, wind velocity, temperature, and greenhouse gas concentrations were conducted, are shown (in Fig. 3a). To obtain the horizontal wavenumber spectra of the fluctuations in the meteorological fields and greenhouse gas concentrations, the almost horizontal segments without sharp course changes and with slightly changing altitude (labeled 1 and 2 in Fig. 1a) were chosen, The average altitude was 9544 ± 34 m for the first segment, and

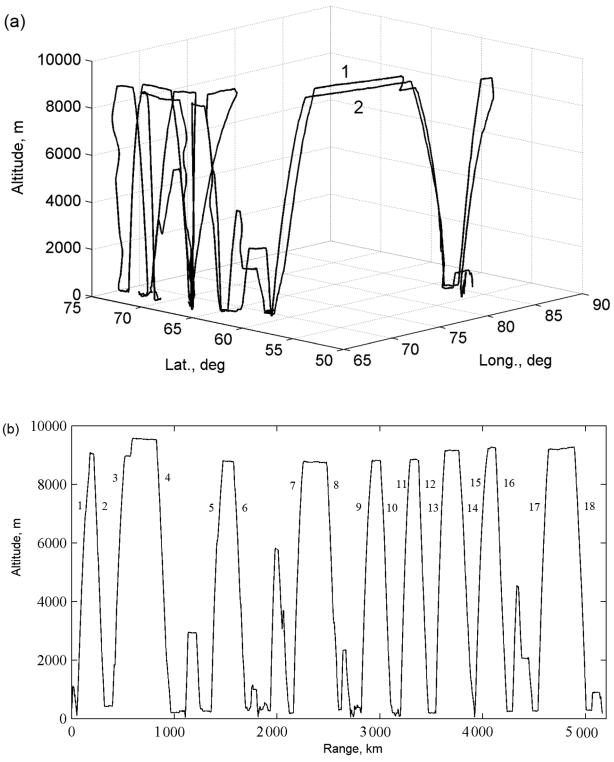

FIG. 1. (a) Aircraft flight path in coordinates of latitude, longitude, and altitude, and almost-horizontal sections of the aircraft flights (segments 1 and 2), along which the measurements of flight altitude, wind velocity, temperature, and greenhouse gas concentrations were conducted; (b) inclined tracks along which measurements were taken.

9219 ± 59 m for the second segment. The flight along segment 1 took place from east to west at about 0700 UTC 8 September 2022, whereas the flight along segment 2 ran from west to east at about 0800 UTC 11 September 2022.

Based on the latitude and longitude values measured by GPS, the distances between neighboring aircraft measurement points were calculated. Usually, this distance was 190 m, which corresponds to a flight speed of approximately 684 km h^{-1}. To bring the data to a constant measurement step the data interpolation was performed with a distance step of 100 m or spatial sampling frequency of 0.01 m^{-1}. Tables 1 and 2 shows the measured gas components and meteorological parameters (atmospheric pressure, temperature, humidity, wind velocity), the instruments used for measurement, and measurement errors.

The details on the instruments and methods for measuring concentrations of different gases using the airplane laboratory, including data on the calibrations of different instruments, are available in Antokhin et al. (2012) and Belan et al. (2022), where the scheme and device for air intake, instruments, and methods for measuring the properties of aerosols, as well as a gas analysis complex are considered. Particularly, the air intakes on the shell of the Tu-134 and the duct layout inside the aircraft are shown in Antokhin et al. (2012, Figs. 4 and 5). The measurement errors are given as well.

The polytetrafluoroethylene tubing with an outside diameter of 6.35 mm and an inside diameter of 4.76 mm fixed inside the inlet spigots [see Fig. 6 in Antokhin et al. (2012) and Fig. 3 in Belan et al. (2022)] was used to deliver the air sample from the intakes to gas analyzers designed to measure O_3, NO_x, and SO_2 gas concentrations. In these works the methods of measuring concentrations of different gases, errors, and frequencies of measurements are given. In particular, the measurement step for the gas concentrations was 1 s and exceeded the time constant of the setup. At average airplane ground speed of 190 m s^{-1} the spatial step of measurements was approximately 190 m, which allowed us to give reliable estimates of spectral density of gas concentration fluctuations at spatial frequencies below $1/(2 \times 190\ \text{m}) = 0.0026\ \text{m}^{-1}$ (i.e., at periods above 380 m).

The wind velocity was calculated using the so-called navigation triangle described in Belan et al. (2022), where in their Table 4 are given the accuracies for determining the parameters included in the navigational triangle. From the navigational triangle, the wind velocity vector was determined as the difference between the aircraft's ground velocity vector (relative to the ground) and the aircraft's velocity vector relative to the air. Thus, the wind vector is a small correction between these very large values resulting in fairly large errors [5% for wind velocity and 10° for wind direction according to Antokhin et al. (2012)]. To calculate the aircraft velocity vector using hemispherical pressure receivers the aerodynamic angles of the airflow over the aircraft were measured. The airspeed of the flow was determined from the difference between the dynamic and static pressures at the flight altitude.

To measure airspeed the manometers are used in combination with a Pitot tube. This tube has a hole with the axis parallel to the longitudinal axis of the airplane toward the incoming airflow. Other holes are located on the side of the tube where the pressure is equal to the static pressure. The difference between the dynamic and static pressures in the Pitot tube is proportional to the square of the velocity of the oncoming flow. The

TABLE 1. Measured gas constituents, instruments/sensors, measurement errors, and time constants.

Block	Device	Parameter	Range	Accuracy	Time constant
Gas analysis complex	Analyzer model 42i-TL	NO_x	0 … 1000 ppb	±1%	60 s
		SO_2	0 … 100 ppm	±1%	60 s
	TEI model 49C	O_3, ppm	0 … 200	0.001 ppm	4 s
	TEI model 48C	CO, ppm	0 … 1000	±1%	1 s
	LI-6262	CO_2, ppm	0 … 1000	<0.2 ppm	1 s
	ME 9850B	SO_2, ppm	0 … 20	±1%	<20 s
	Model CLD 780 TR	NO_x, ppm	0 … 0.5	<0.003 ppm	1 s

TABLE 2. Measurements of meteorological parameters, instruments/sensors, units, and accuracy (time constant 1 s and measurement step 1 s).

Parameter (device)	Units	Accuracy
Flight altitude, by static pressure (electromechanical altimeter VEM-72)	m	10 m
Air temperature (HYCAL Sensing Products Honeywell Inc., model: IH-3602C)	°C	0.5°C, with step 0.1°C (− 70 … +70)
Full braking air temperature (resistive-type sensor)	°C	0.5°C
Relative humidity (HYCAL Sensing Products Honeywell Inc., model: IH-3602C)	%	7% c with step 1% (0 … 100)
Atmospheric pressure (Motorola MPX4115AP)	mm Hg	1.5%,100–860 mm Hg
Aircraft speed (DISS-3A "Strela")	km h^{-1}	1 km h^{-1}
Aircraft speed relative to the air	km h^{-1}	1 km h^{-1}

Pitot tube is used to measure the projection of wind velocity on the direction of flight.

The velocity vector of the aircraft relative to the ground was calculated from the inertial navigation systems and GPS global positioning systems. All the air navigation data were received from the KompaNav-5.2 navigation system (http://www.teknol.ru) supplemented by the Airborne Signal System (ASS). The ASS obtains the airspeed from the dynamic and static pressures as described above, and barometric altitude of the airplane.

4. Results of measurements of horizontal fluctuations of wind velocity and greenhouse gas concentrations: Their horizontal spectra and structure functions

a. Measurements and horizontal wavenumber spectra in the upper troposphere (heights 9–10 km)

The results of measurements of flight altitude, variations of meridional (mw) and zonal (zw) components of wind velocity, temperature, and concentrations of some greenhouse gases (NO and NO_2) in 2022 (segment 1) are shown in Fig. 2, whereas the results of similar measurements conducted in 2020 are shown in Fig. 3. Vertical velocity components have not been measured. From the measurements of wind velocity vector described in section 3 we also calculated its meridional and zonal components. The variations of gas concentrations are normalized to their rms values (designated by std and indicated on the plots) for ease of comparison of all variations.

To estimate the spectral density of the measured fluctuations the standard Welch method was used. This estimate was obtained by moving a sliding window along the overlapping data sample. The length of the analysis window was usually chosen to be 200 km, which was sufficient to estimate the spectral density for spatial periods of about 100 km and below. After interpolating the data with a step of 100 m the highest spatial frequency of the obtained spectra was 10 km^{-1}. However, since the real step of measurements was approximately 190 m, the

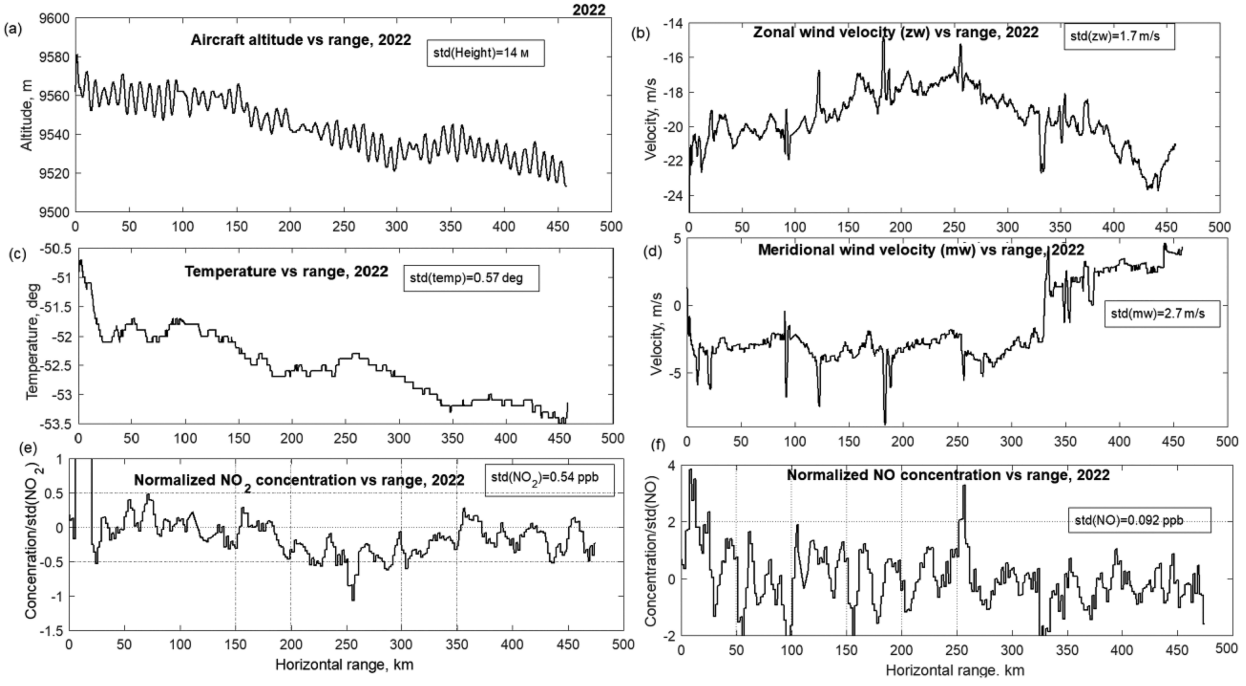

FIG. 2. Horizontal variations of (a) flight altitude, (c) temperature, (b) zonal (zw) and (d) meridional (mw) components of wind velocity, and (e) NO_2 and (f) NO concentrations from measurements in 2022 (segment 1).

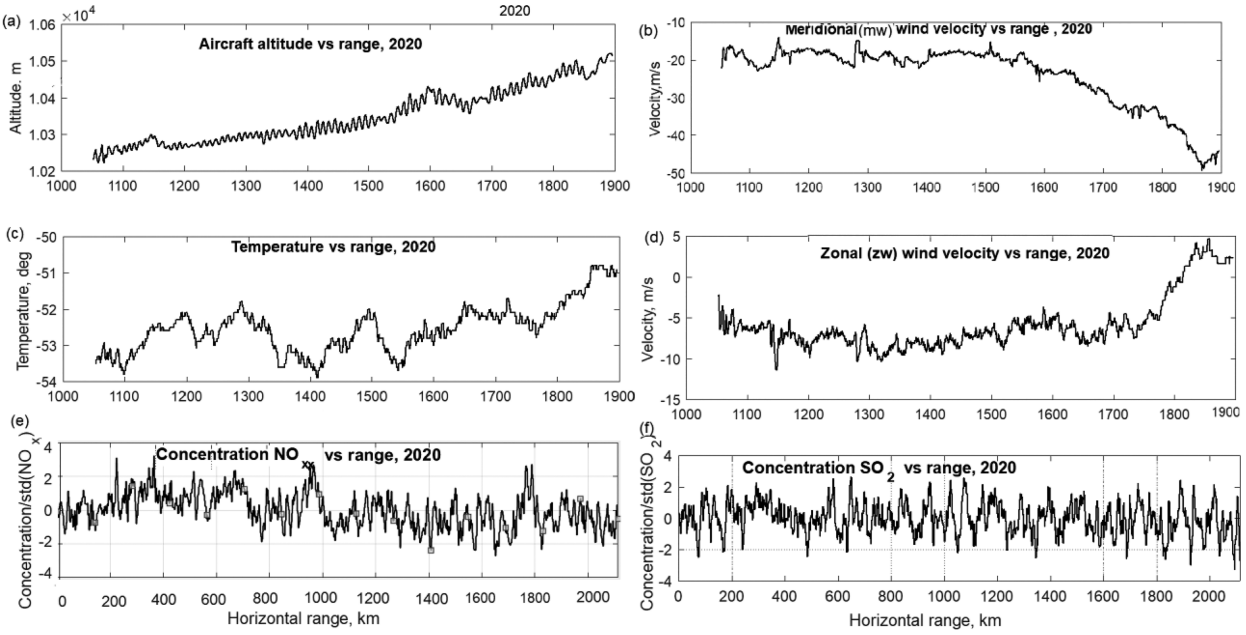

FIG. 3. Horizontal variations of (a) flight altitude, (b) meridional wind velocity (mw), (c) temperature, (d) zonal wind velocity (zw), (e) NO_x concentration normalized to std(NO_x) = 0.0117 ppb, and (f) SO_2 concentration normalized to std(SO_2) = 0.0756 ppb, obtained from aircraft measurements in the Arctic region in 2020.

obtained spectra should be considered up to frequencies of 2.63 km^{-1}, or periods $190 \times 2 = 380$ m.

To reduce the influence of edge effects on the spectral density estimation, the removal of the mean and weighting of the data with the Hamming window was applied. The overlap of the windows was 80%. Before calculating spectral density of fluctuations, they were normalized to their standard deviations, so that it was convenient to compare the spectral densities of fluctuations of different meteorological parameters and gas concentrations.

Figure 4 shows estimates of the spectral densities of variations in the horizontal wind velocity E_k, [the E_k spectrum is obtained by adding the spectra of zonal (zw) and meridional (mw) wind velocity components, actually being a spectrum of kinetic energy per unit mass], temperature (temp), and gas concentrations NO_2 and NO for segment 1 (Fig. 4a) and segment 2 (Fig. 4b), normalized to the corresponding variances of the variations. It can be seen from Fig. 4a that at scales less than 6 km the experimental spectra show a tendency to increase the slope, compared to the slopes of the spectra at scales of more than 6 km.

To compare the obtained spectra with theoretical ones we take into account that the main parameters in our model are the rms value of wind velocity fluctuations σ, the Brunt–Väisälä frequency N, the inertial frequency f, and the ratio of rms values of horizontal wind velocity fluctuations to vertical ones, $\chi = \nu_1/\nu_V = \sigma/\sigma_V$. For the measured wind velocity fluctuations along segment 1, the value σ was about 3 m s^{-1}, and the average value of the Coriolis parameter $f = 1.25 \times 10^{-4}$ rad s^{-1} in the latitude range (56°–60°), where the flight took place.

As for the average values of the buoyancy frequency N in the upper tropospheric layer, they can be estimated from radiosonde data in the nearest to segment 1 (see Fig. 1a) cities Kolpashevo (58°18′47″N, 82°54′32″E) and Tobolsk (58°11′53″N, 68°15′16″E) (Fig. 5). One can see from Figs. 5c and 5d that the wind velocity components in the tropospheric layer 9.5–10 km vary very weakly with height: their vertical gradient is less than 2(m s^{-1}) km^{-1}. The change in the N^2 in the same layer is within the interval (1–9) $\times 10^{-4}$ rad^2 s^{-2}; therefore, $N = 0.02$ rad s^{-1} can be taken as a mean value in the layer.

From the measurements of vertical and horizontal velocity fluctuations in the upper troposphere by Lilly and Lester (1974) and Nastrom et al. (1987) it follows that the typical values of χ in the stably stratified upper troposphere can lie in the range (2–5).

At $k > k^* = 2\sqrt{e_0}m^*$ our model predicts a steeper decay ($\sim k^{-3}$) of the spectral density with increasing k compared to the spectrum of Nastrom and Gage (1985) lying at longer horizontal scales ($k < k^*$). The parameter $e_0 \sim M^2/(8\chi^2) \ll 1$ characterizes the anisotropy of similarly shaped thin-layered inhomogeneities with scales less than the outer horizontal scale

$$L^* = 2\pi/k^* = 2\pi/(2\sqrt{e_0}m^*) \approx 2\sqrt{2}\pi\sigma\chi/(MN). \quad (5)$$

As can be seen from (5), the scale L^* depends on the nonlinearity parameter M, frequency N, and parameters χ and σ. Taking $\chi \sim 2$, $N = 0.02$ rad s^{-1}, $M = 0.4$ (under nonlinear saturation of the spectrum) and $\sigma = 3$ m s^{-1} we can estimate $e_0 \sim 0.005$, and $L^* \sim 6$ km, as follows from (5). At scales less than L^* our model predicts a rapid spectrum decay (−3) with decreasing horizontal scales. For $f = 1.25 \times 10^{-4}$ rad s^{-1}, $\sigma = 3$ m s^{-1}, an estimate of the energy generation rate gives $\varepsilon_g \equiv \sigma^2 f = 0.0011$ m^2 s^{-3}. The horizontal spectrum of wind velocity fluctuations obtained from (4) using the parameters

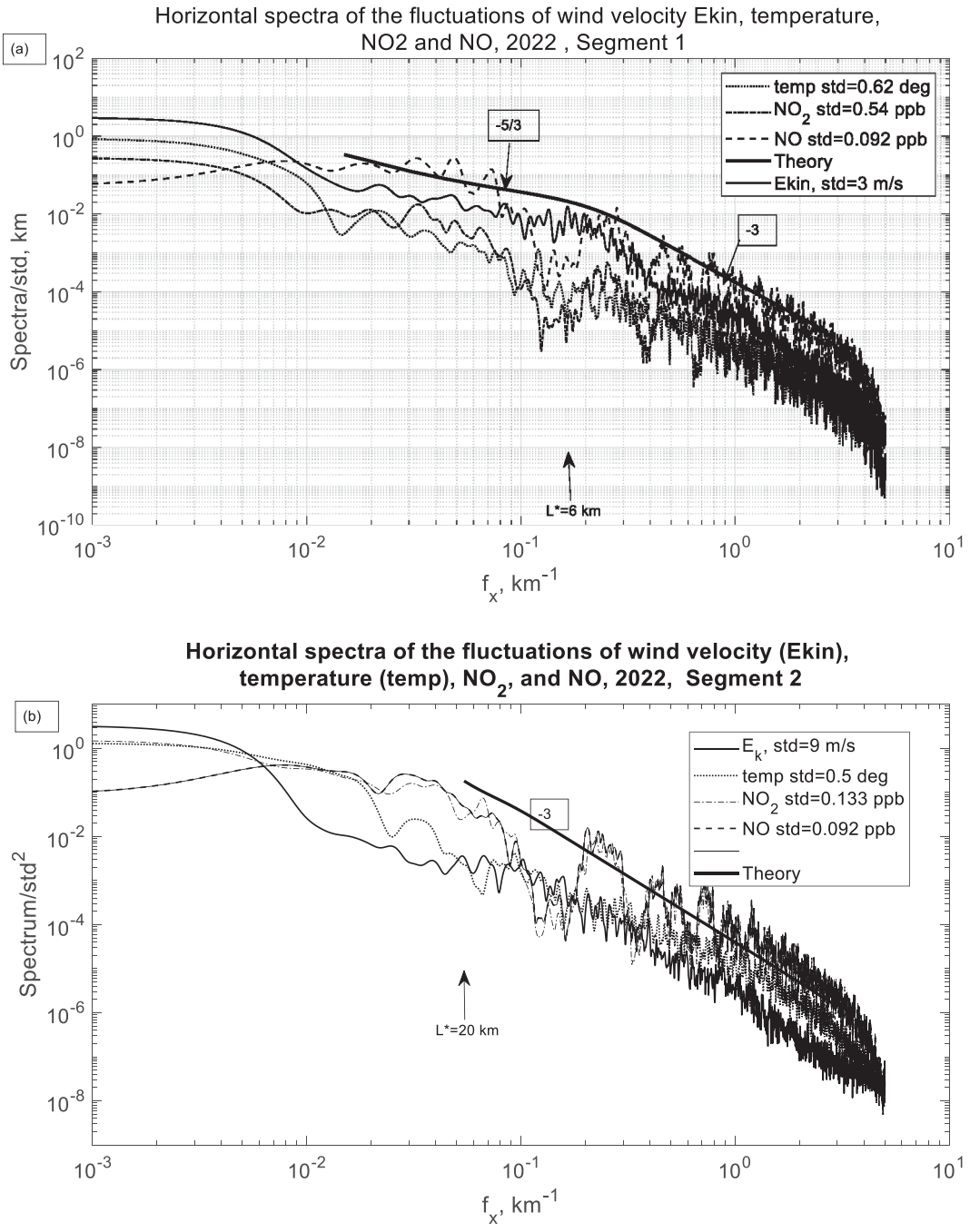

FIG. 4. Horizontal spectra of variations in the horizontal wind velocity E_k, temperature (temp), and concentrations of NO_2 and NO gases for (a) segment 1 and (b) segment 2, normalized to the corresponding variances of these variations. The bold line corresponds to the theoretical spectrum given by (4), which has a high-wavenumber spectrum section with a slope of -3 and an outer horizontal scale L^*.

estimated above and normalized to the variance $\sigma^2 = 9\ \mathrm{m^2\ s^{-2}}$ is shown by the bold line in Fig. 4a.

The individual spectra in Fig. 4a have a "comblike" shape with a large number of spectral maxima and minima. Among them, the spectrum of wind velocity fluctuations E_k does show an increase of its slope at scale $L^* \sim 6$ km , when passing through this scale and further scale decreasing. In the other individual spectra such a transition is less pronounced than in the spectrum E_k. Nevertheless, their average slope at short scales, from $L^* \sim 6$ km to 400 m, is closer to the theoretical

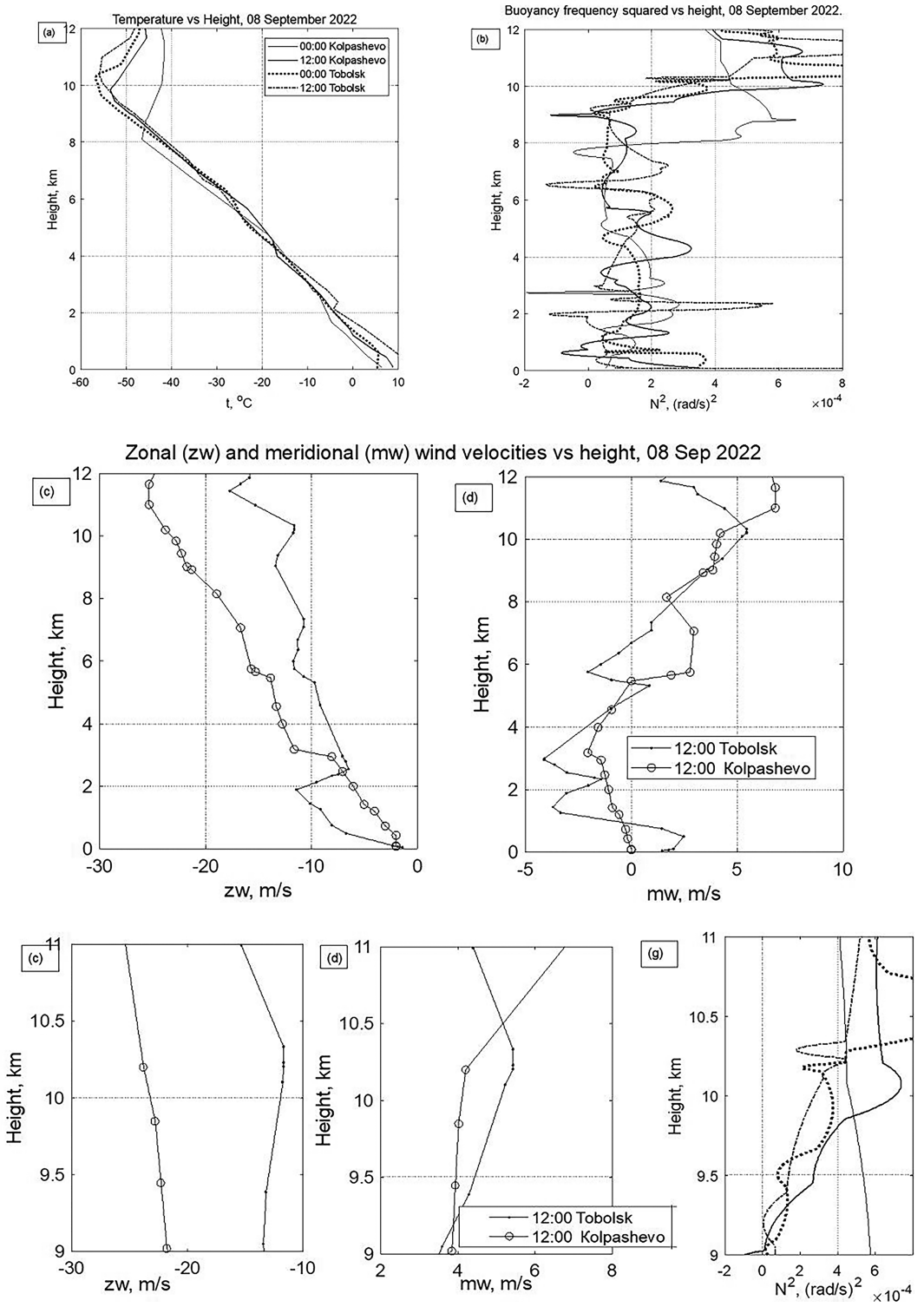

FIG. 5. Vertical profiles of zonal (zw) and meridional (mw) components of wind velocity, temperature (t), and Brunt–Väisälä frequency squared (N^2), obtained from radiosonde data in Kolpashevo (58°18′47″N, 82°54′32″E) and Tobolsk (58°11′53″N, 68°15′16″E). on 8 Sep 2022, when the flight along segment 1 took place.

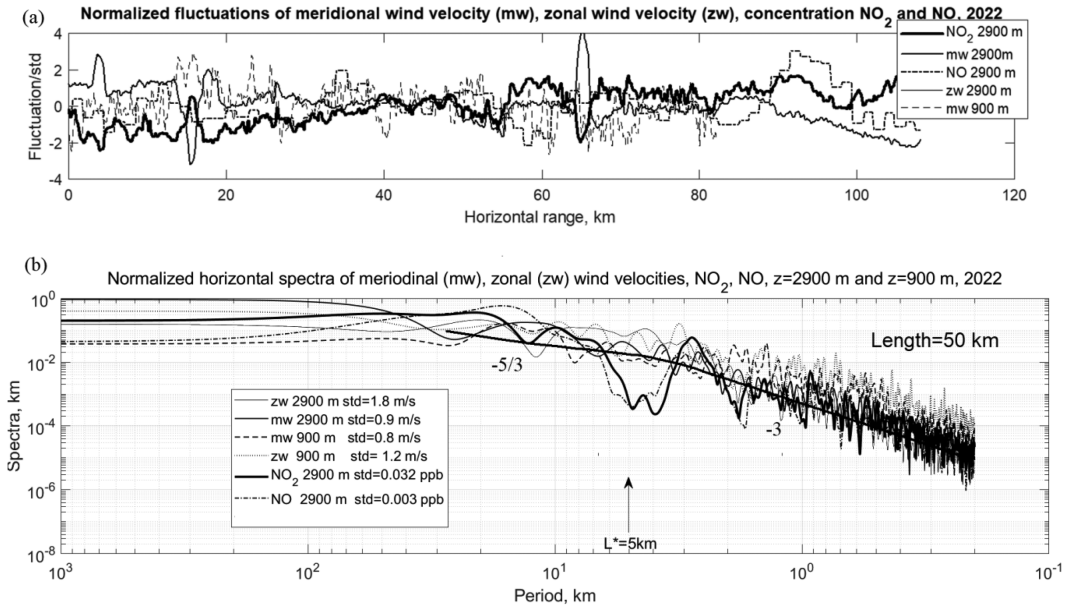

FIG. 6. (top) Measured fluctuations of the meridional (mw) and zonal (zw) components of wind velocity, and gas (NO and NO_2) concentrations at heights of 900 and 2900 m and (bottom) their horizontal spectra.

slope −3 (Fig. 4a) than to the −5/3 slope of the experimental spectra obtained by Nastrom and Gage (1985).

The increase of the spectral slope was also observed for gas tracers, what can be expected from the relation (3b) between wavenumber spectrum of gas concentration fluctuations q and wind velocity spectrum. Bacmeister et al. (1996) observed the slope increase only in the wind velocity horizontal spectrum, but not in the horizontal spectra of gas tracers. The latter depend on the vertical gradients of mean gas concentrations dq_0/dz [see expression (3b)], so if the vertical scale of change of the mean gas concentration is much greater than the amplitudes of displacements, then the relative fluctuations of gas concentrations will be small compared to 1. The smallness of change of q_0 on the vertical distance of order air parcel displacements leads to the absence of the steep section in the horizontal spectra of gas tracers. Since the data on the average gradients of gas concentrations were not given by Bacmeister et al. (1996) the reasons for the absence of a steep section of the spectrum in this work remain unknown.

When flying along segment 2, the value of σ was about 9 m s^{-1}, i.e., 3 times higher than that along segment 1. For segment 2 the estimate of the characteristic horizontal scale L^* gives values of 18–20 km, so the model predicts a transition to a steep spectrum on a much longer scale than in the case of measurements along segment 1. The spectra in Fig. 4b did have a slope close to −3 for periods of less than 20 km. The existence of the transition on some scale L^* from shallow to steeper spectrum is also confirmed below by the results of our measurements in September 2022 at lower heights of 900 and 2900 m carried out under stable stratification of the lower troposphere inherent the Arctic region.

b. *Measurements and spectra along short horizontal traces (lengths of about 50 km) at heights of 900 and 2900 m of the lower troposphere*

The results of measurements of the fluctuations of the meridional (mw) and zonal (zw) components of wind velocity and gas concentrations (NO and NO_2) along short horizontal segments of about 50 km long, located at altitudes of 900 and 2900 m, and their horizontal spectra are shown in Fig. 6. The analysis of the N^2 profile in the layer 900–2900 m indicates the presence of stable temperature stratification of the troposphere ($N^2 > 0$) during the measurement periods (Fig. 5b). The exceptions are thin layers less than 100 m thick located at heights of about 2600, 1900, and 500 m, where the local N^2 values were negative at certain time intervals, suggesting the occurrence of convective instability in these layers. As in the case of flights at heights above 9 km, the experimental spectra obtained at heights of 900 and 2900 m (Fig. 6, bottom panel) indicate an increase in the slope of the spectra at scales less than $L^* \sim 5$ km.

c. *Comparison with measurements in 2020*

To make sure that the transition from the −5/3 spectrum to a steeper spectrum was observed not only under the conditions of stable tropospheric stratification developed exclusively in September 2022, we compared our 2022 measurements with the results of similar airplane measurements in the Arctic region carried out in September 2020. In 2020 the components of wind velocity, temperature, and concentrations of NO_x, SO_2, and other gases (shown in Fig. 3) were measured at altitudes of 10.3–10.5 km. The temperature and wind profiles (not shown here) obtained from radiosonde data in cities close to the flight segment (Norilsk, Naryan-Mar, and Arkhangelsk) indicated stable stratification of the troposphere at flight heights. In 2020 these heights were below the tropopause

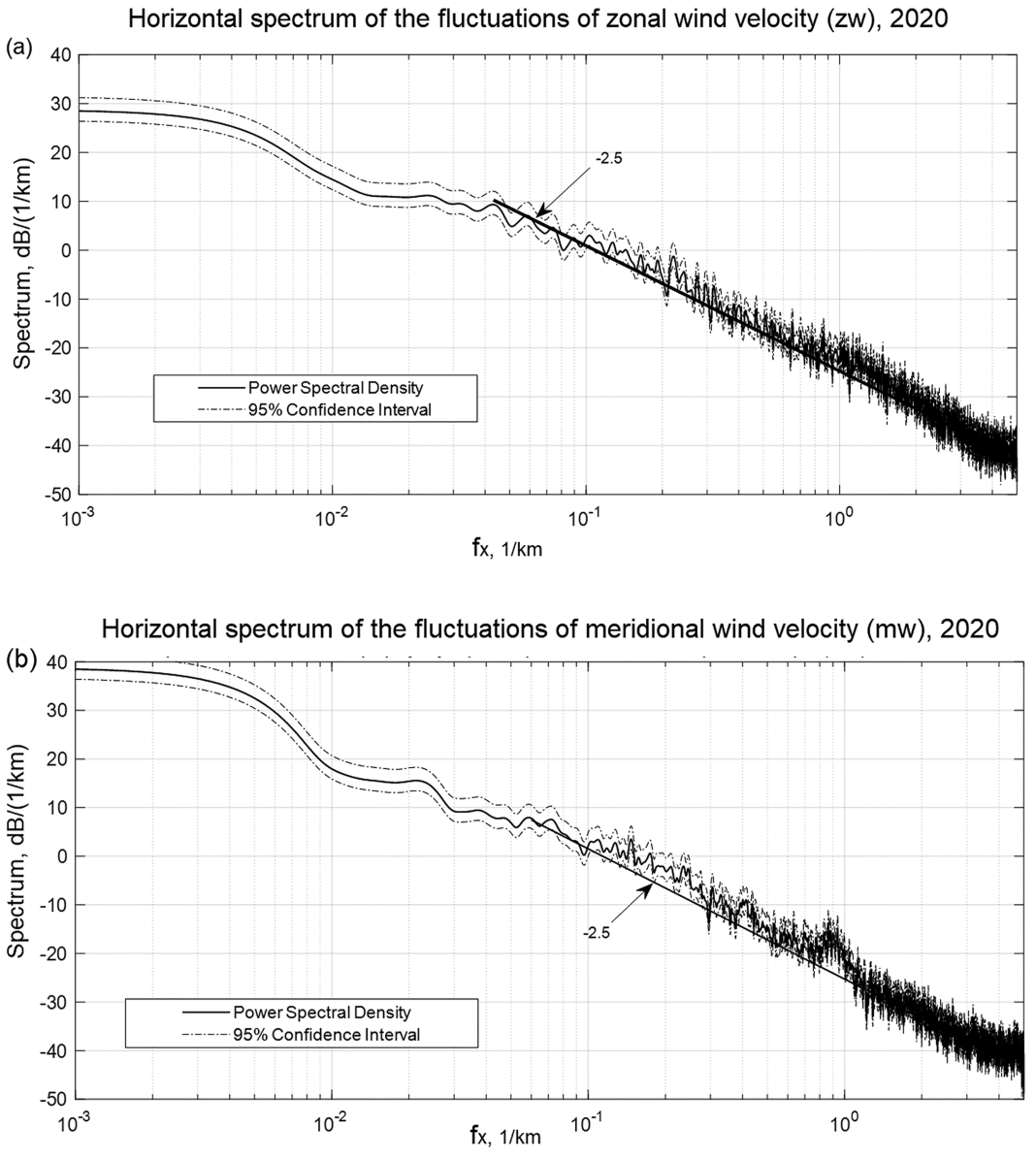

FIG. 7. Horizontal spectra of the fluctuations of (a) zonal (zw) and (b) meridional (mw) wind velocity components measured in September 2020 (in Figs. 4b,d). The dotted lines show the 90% confidence intervals of the spectral estimates.

(heights of 12–14 km) for Naryan-Mar and Arkhangelsk, and in the tropopause for Norilsk (heights of 9–11 km).

The obtained spectra of the fluctuations of meridional (mw) and zonal (zw) wind velocity components at a flight altitude of about 10 km are shown in Fig. 7, where $f_x = k_x/2\pi$, and k_x is the horizontal wavenumber. The slopes of these spectra for short periods from 400 m to 10 km are ranging from −2.5 to −2.7. Approximately the same slopes in the same range of periods were obtained for the spectra of fluctuations of concentrations of NO_x, SO_2, CO_2, and O_3, shown in Fig. 8. These slopes are not as steep as predicted by the theoretical −3 law, but are closer to it than to the −5/3 spectrum of Nastrom and Gage (1985), which the current models of horizontal spectrum formation aim to explain (Lindborg 2006, 2015; Callies et al. 2014; Skamarock et al. 2014).

d. *Horizontal structure functions of the measured fluctuations of meteorological parameters and gas concentrations*

The obtained spectra of the fluctuations of meteorological parameters and gas concentrations are connected with the structure functions of these fluctuations defined by the mean square $\langle [T(x_2) - T(x_1)]^2 \rangle$ of the difference of the fluctuations of any parameter $T(x)$ in two arbitrary points with horizontal coordinates x_1 and x_2. For homogeneous random processes, and processes with stationary increments, the second-order

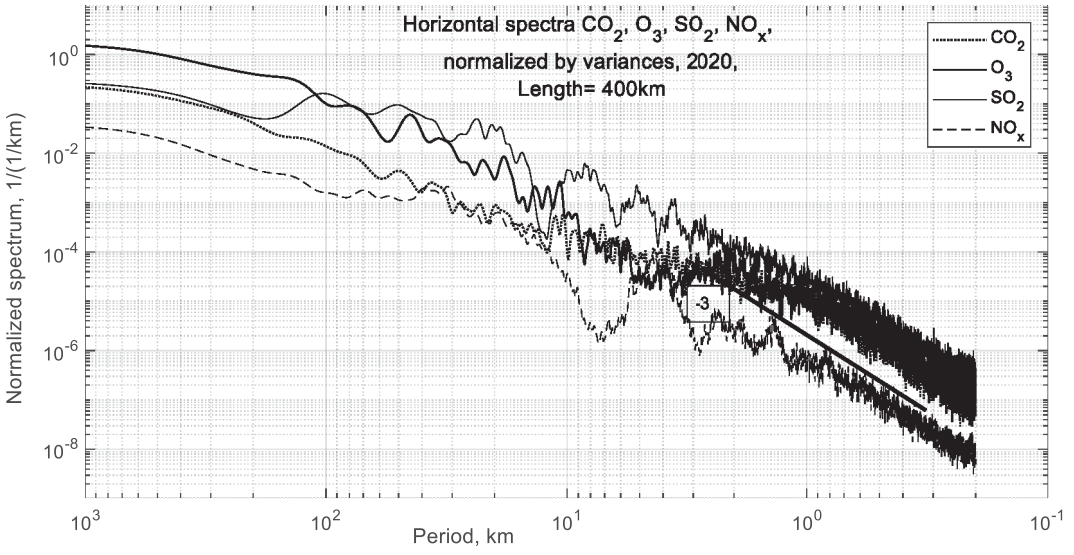

FIG. 8. Horizontal spectra of fluctuations in the concentration of CO_2, O_3, SO_2, and NO_x obtained in September 2020 at a flight altitude of about 10 km. The solid line shows the −3 spectrum predicted by the theory at short wavelengths from 400 m to 10 km.

structure function $D(R)$ depends only on the coordinate difference $R = x_2 - x_1$ and is expressed through the correlation function $B(R)$ of the random process $T(x)$ as follows:

$$D(R) = 2[B(0) - B(R)]. \quad (6)$$

For a structure function of the form $D(R) \sim R^{\gamma}$ with a power $\gamma > 0$ the corresponding spectrum is $E(k) \sim 1/k^{\gamma+1}$ (see Monin and Yaglom 1975; Golitsyn 2012).

Using the measured data, we first calculated the autocorrelation function $B(R)$ for the selected flight segment and then calculated the structure function using formula (6). The resulting structure functions of the meridional (mw) and zonal (zw) wind velocity fluctuations for segment 1 (2022) in the range of scales R from 400 m to 150 km are shown in Fig. 9.

As the scale R grows from 400 m to $L^* \sim 6$ km, there is a rapid growth of structure functions along with R proportionally

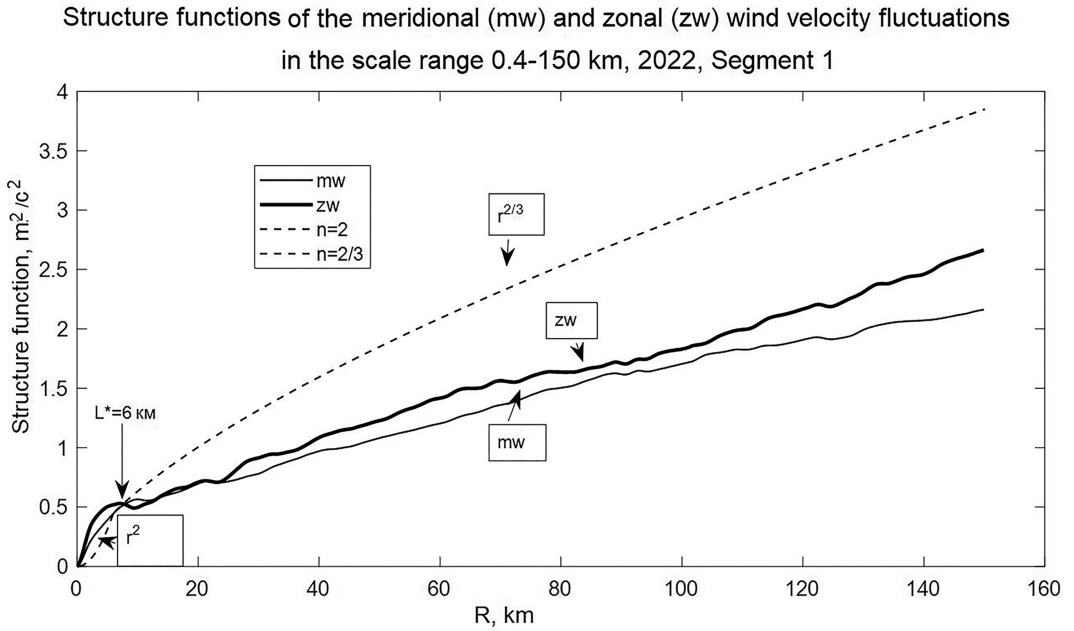

FIG. 9. Horizontal structure functions of the meridional (mw) and zonal (zw) wind velocity fluctuations in the scale range 0.4–150 km.

to R^{γ} with $\gamma = 1.1$–1.2. As we move to larger scales $R > L^*$, the growth slows down strongly ($\gamma = 0.6$). Compared to the observed growth the model (dashed line in Fig. 9) predicts faster growth ($\sim R^2$) of the structure function with increasing scales from 400 m to $L^* \sim 6$ km and in the large-scale region ($\sim R^{2/3}$) at $L^* < R < 150$ km.

Nevertheless, a noticeable decrease in the growth rate γ of the structure function when moving from scales of 400 m $< R < L^*$ to larger scales $R > L^*$ confirms our conclusion about the presence in the spectrum E_{kin} (Fig. 4a) of a transition at scales on the order of L^* to a steeper spectrum (compared with the $-5/3$ law).

A decrease in the growth rate was also observed for the structure functions of the fluctuations in the concentration of some greenhouse gases (NO, NO_2) in 2022 (Figs. 10a,b), and (NO_x, SO_2) in 2020 (Figs. 10c,d) in the transition from short scales 400 m $< R < L^*$ to longer ones with $R > L^*$.

It is necessary to note that it was in the Arctic experiment under conditions of stable stratification of the troposphere that we were able to detect the presence of a range of short scales of 400 m $< R < L^*$ for the fluctuations of greenhouse gas concentrations, in which the growth rate of structure functions is higher than 2/3, while the degree of decay of horizontal spectra is closer to -3, rather than to $-5/3$. The presence of this scale range in the stably stratified troposphere should be taken into account when calculating the dependence on the scale R of the horizontal turbulent diffusion coefficient of passive tracers, which is proportional to the product of R by the square root of structure function of horizontal velocity fluctuations (Monin and Yaglom 1975; Golitsyn 2012, chapter 6).

5. Slanted spectra

In addition to horizontal fluctuation spectra the information about 3D spatial structure and anisotropy of the fluctuations of wind velocity, temperature, and gas concentrations in the troposphere can be obtained by measuring these fluctuations along aircraft tracks inclined to Earth's surface. Such measurements of temperature fluctuations were first carried out by Gurvich and Kukharets (2008) over northern regions of the European part of Russia under stable stratification of the troposphere in the height range of 2–8 km. The obtained slanted and horizontal spectra of fluctuations covered the range of wavenumbers from 5×10^{-4} to 3×10^{-2} rad m^{-1}, which corresponded to scales from 12.6 km to 200 m. These spectra were interpreted with a model of 3D spectrum of temperature inhomogeneities generated by a statistical ensemble of internal waves (Gurvich and Chunchuzov 2008), and using a single set of model parameters. It turned out that the slanted spectra in some range of wavenumbers approach the -3 power law with a small deviation in the region of large wavenumbers. Estimates of the parameters of the 3D spectrum showed the presence of similar in shape and strongly elongated along Earth's surface temperature inhomogeneities with vertical scales over 100 m and horizontal scales 20 or more times greater than the vertical scales. However, when the vertical scales decreased to 10–20 m, the anisotropy of inhomogeneities (ratio of horizontal sizes to vertical ones) decreased to 1.5–2.

A decrease in the anisotropy of temperature inhomogeneities with decreasing scales was also observed in the spectra of star scintillations obtained from space (Kan et al. 2014). At stratospheric heights of 30–43 km, the anisotropy of temperature inhomogeneities was found to decrease from about 50 to 10 as the vertical scales decrease from 55 to 8 m.

In the present experiment the spectra of fluctuations of temperature, wind velocity, and NO concentration were obtained along inclined traces with angles of inclination from 2° to 7° to the ground surface. Figure 11 shows the fluctuations of temperature, NO concentration, and wind velocity components (mw and zw) as a function of the heights of the measurement points (in the height range of 1–9.3 km) on the inclined traces and normalized to the corresponding rms values (std).

If we assume that the inclined route of the aircraft crossed random layered inhomogeneities, which are statistically homogeneous and stationary during the flight times along two sections of the route lying in the height ranges of 1–5 km and 5–9 km, then we can estimate the spectra of these inhomogeneities over the vertical scales (Figs. 12 and 13). The measured temperature fluctuations as a function of altitude are shown in Fig. 12a. Their spectrogram obtained with a sliding analysis window of 3 km (Fig. 12b) shows an increase in spectral density with increasing altitude for $f_z = k_z/2\pi < 5$ km^{-1} (vertical scales above 200 m), where k_z is the vertical wavenumber. Such a growth of the spectral amplitude of the fluctuations with height, and a decrease in the characteristic vertical wavenumber $m^* = 1/(\sqrt{2}\nu_V) = N/(\sqrt{2}\sigma)$ [see (2) and (3)] due to a decrease in mean atmospheric density, is typical for a fine-scale layered structure of the atmosphere (Chunchuzov and Kulichkov 2020, section 5).

Figure 13 shows estimates of the slanted spectra for the fluctuations of the horizontal wind velocity components (mw and zw), temperature, and NO concentration, corresponding to their profiles shown in Fig. 11. The Welch spectra of the wind velocity components (Fig. 13a) were calculated for the altitude ranges of 1000–3048 m and 7100–9148 m with a Hamming window of 512 m. For the lower and upper atmospheric layers, the values of σ are 1.33 and 2.32 m s^{-1}, respectively, and the average N values in these layers lie in the range 0.01–0.02 rad m^{-1}.

Taking for the lower tropospheric layer $N = 0.02$ rad m^{-1}, $\sigma = 1.33$ m s^{-1}, and $\alpha = 0.2$, we obtain the vertical wavenumber velocity spectrum (3) decaying according to the -3 law when increasing vertical wavenumber k_z or $f_z = k_z/2\pi$ (solid line in Fig. 13a). The outer scale bounding this spectrum $L_v = 2\pi/m^* = 600$ m and the critical wave breaking scale $L_c \sim 4$ m are shown by vertical arrows. Estimates of the mw and zw spectra over a range of vertical scales from 600 to 10–20 m show that these spectra decay according to a law close to -3. However, as the scales decrease further ($f_z > 0.1$ m^{-1}), the spectral estimates have false maxima and minima, which appear to be due to almost periodic variations in aircraft altitude by 10–20 m as a function of distance along the track (for the horizontal track these variations can be seen in Fig. 3a).

Estimates of the spectra of temperature fluctuations are shown in Fig. 13b along with the theoretical spectrum (Fig. 3a)

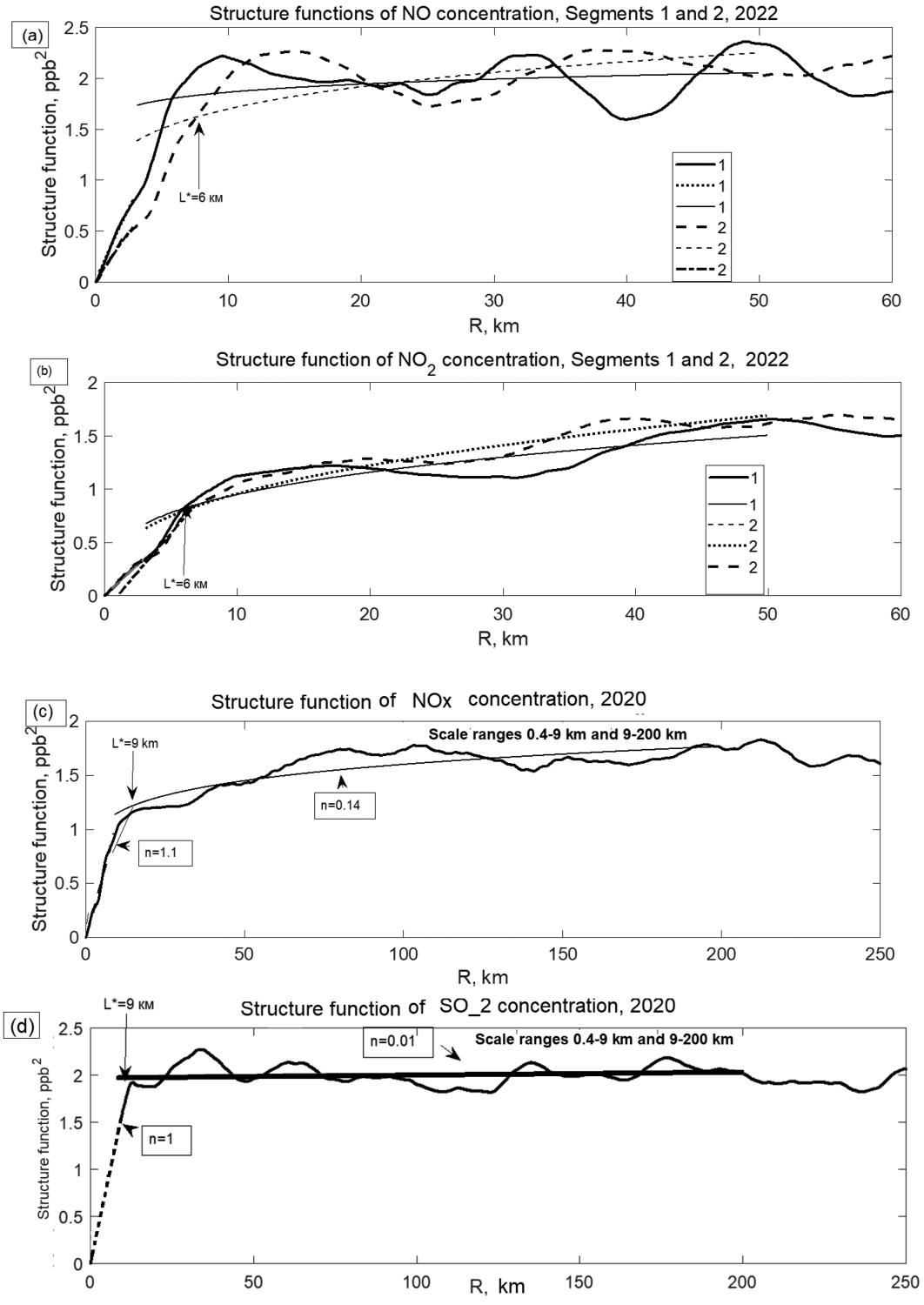

FIG. 10. Horizontal structure functions of the fluctuations of greenhouse gas concentrations of (a) NO and (b) NO_2 in 2022 and (c) NO_x and (d) SO_2 in 2020.

(solid line) obtained for the average temperature $T_0 = 280°$. Although the individual spectra are close to the theoretical one for short vertical scales of 100–10 m, there is a deviation from it at longer periods.

The slope of the individual spectra of NO concentration fluctuations in the scale range from 600 to 20 m is consistent with the slope of the theoretical spectrum (thick line). The latter was obtained from (3b) with an average gradient

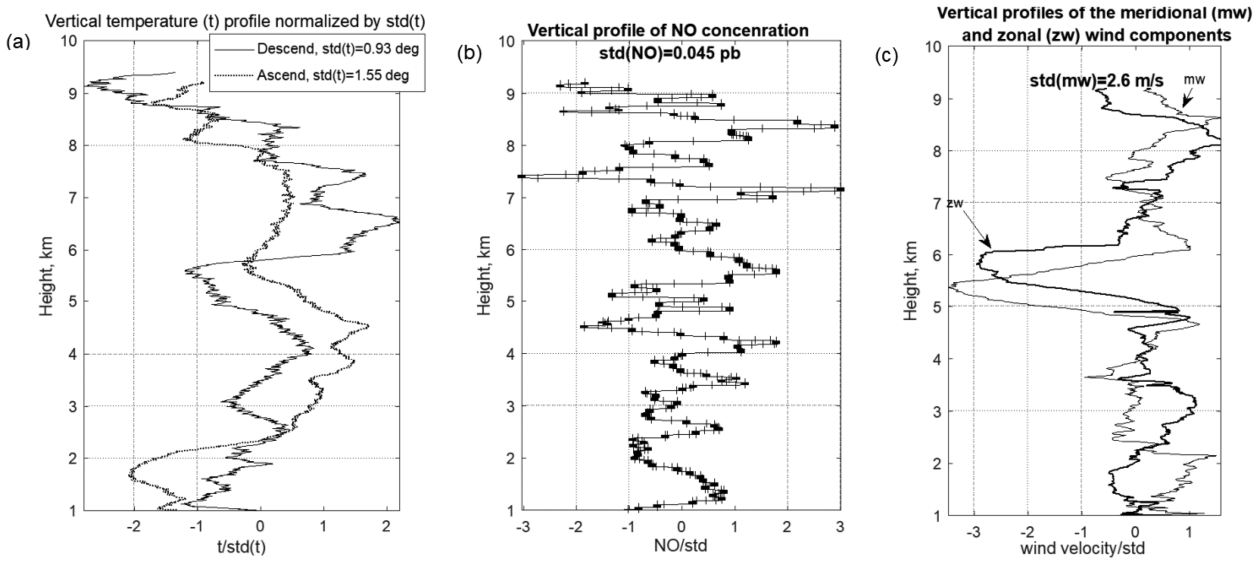

FIG. 11. Vertical profiles of the fluctuations of temperature, NO concentration, and wind velocity components (mw and zw) as a function of the altitudes (1–9.3 km) of measurement points on the slanted traces and normalized to the corresponding rms values (std).

$dq_o/dz \sim 0.008$ ppb km^{-1} of NO concentration estimated from the obtained NO profile. Such behavior of the spectra of wind velocity and NO concentration fluctuations in a certain range of scales suggests a significant influence on the formation of these spectra of the process of advection of air particles induced by internal waves and vortical motions. The average vertical wavenumber spectrum of velocity fluctuations (Fig. 13d) obtained during descents and ascents of the aircraft along different inclined routes (shown in Fig. 1), decreases according to the law close to -3 when decreasing the vertical scale from 300 to 30 m (straight line in Fig. 13d).

The vertical spectra of horizontal wind velocity fluctuations in the stably stratified troposphere obtained from airborne measurements along inclined tracks agree well with similar spectra in the upper troposphere and stratosphere obtained from numerous radar measurements (Fritts et al. 1988; Fritts and Alexander 2003) and infrasound sounding data (Chunchuzov and Kulichkov 2020, section 6).

Our conclusion about the significant influence of the internal wave-induced advection on the formation of the vertical wavenumber spectra of greenhouse gases confirms the results of Yuan et al. (2009), who obtained from ozone-probe measurements the vertical profiles of ozone concentration in the troposphere and lower stratosphere, and vertical wavenumber spectra of ozone concentration fluctuations. The average slopes of these spectra in the wavenumber range from 4.69×10^{-4} to 2.50×10^{-3} m^{-1} (the corresponding vertical scales are between 2 km and 400 m) were about -2.91 in the

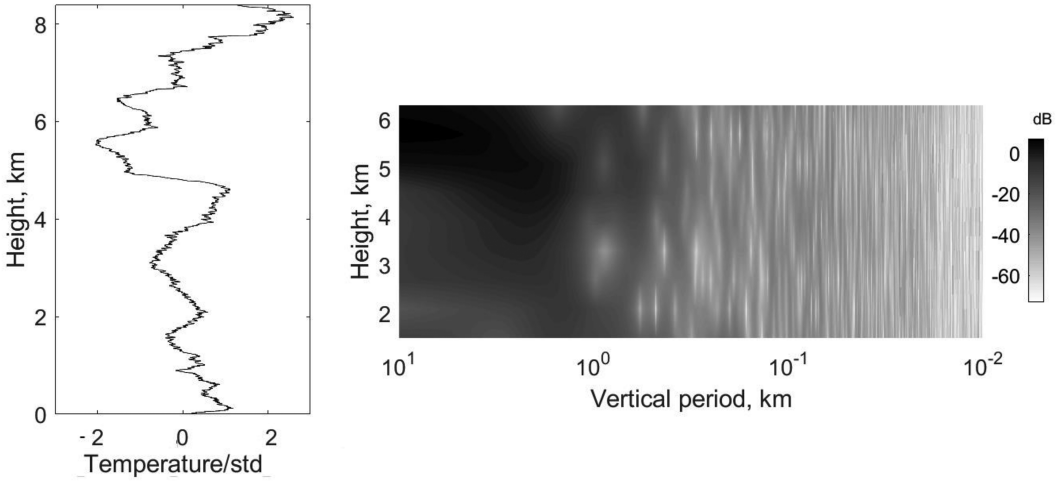

FIG. 12. (left) Vertical profile of temperature fluctuations after trend removal, normalized to rms value, and (right) its spectrogram.

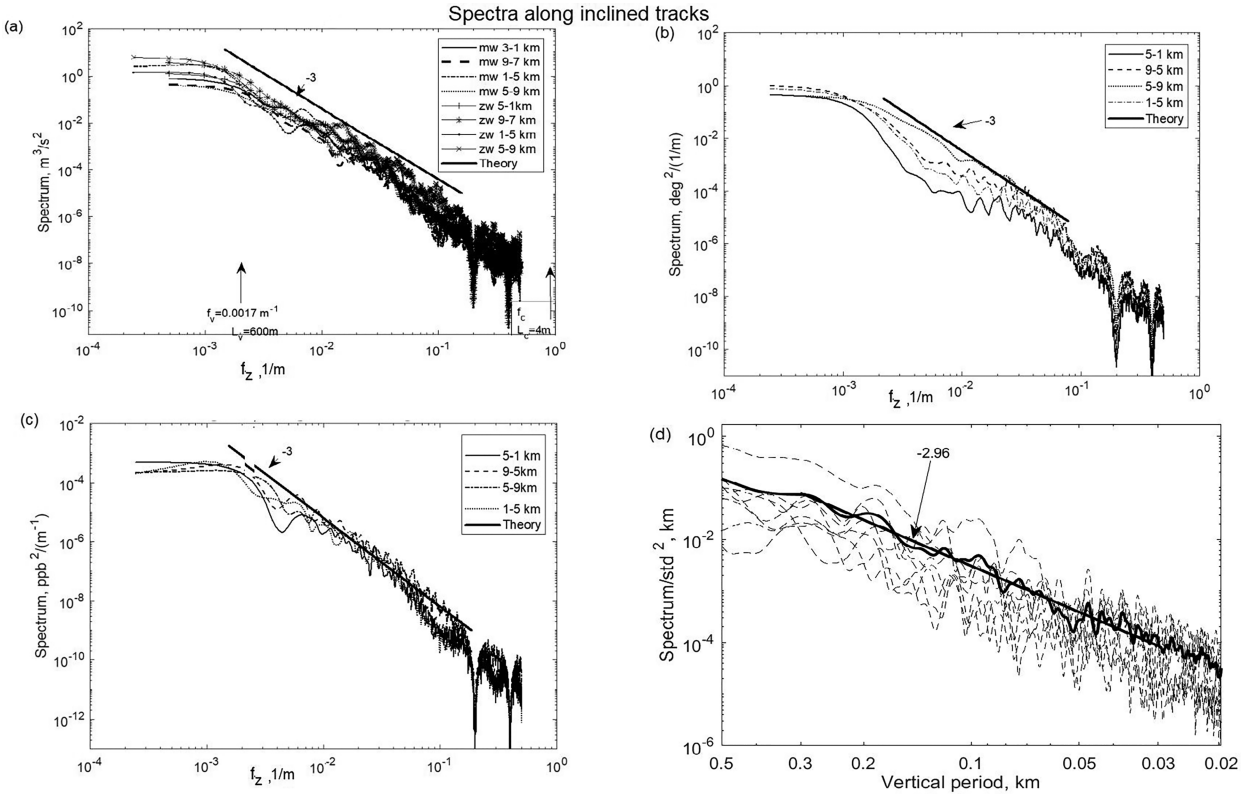

FIG. 13. Vertical wavenumber spectra of the fluctuations of the horizontal components of (a) wind velocity (mw and zw), (b) temperature, and (c) NO concentration, measured along inclined routes during the descent and ascent of the aircraft. The horizontal axis is a spatial frequency $f_z = k_z/2\pi$ in cycles m^{-1}, where k_z is the vertical wavenumber. The altitude ranges for which the spectra were calculated and the theoretical spectra with a slope of −3 (straight line) are indicated. (d) Individual spectra of mw for different traces at ascents and descents, their average spectrum (thick curve), and its approximation in the range of vertical scales from 300 to 30 m (straight line with a slope of −2.96).

troposphere, and −2.87 in the lower stratosphere, which were close to the −3 slope. From the agreement of the observed and theoretical spectra a conclusion was made by Yuan et al. (2009) about a significant contribution of the IGWs to the observed fluctuations of ozone concentrations in the troposphere and lower stratosphere.

6. Conclusions

We presented in this paper the results of airborne measurements with the aircraft laboratory Tu-134 "Optik" of the mesoscale fluctuations of wind velocity, temperature, and concentrations of gas constituents at different heights of the troposphere of the Arctic region of Russia. The obtained statistical characteristics of the fluctuations (spectra and structure functions) were interpreted using a theoretical model of the formation of mesoscale wind velocity and temperature fluctuations described in the paper. It is important to note that this model takes into account the influence of advection of each internal wave or vortex by the varying wind field induced by all the other waves and vortexes on the fluctuation spectrum formation. Such an advection becomes significant at certain short horizontal and vertical scales comparable with the corresponding rms displacements of the air particles. It follows from the model that in a stably stratified atmosphere, the energy of internal waves and horizontal vortical motions, generated by their random sources on some characteristic vertical and horizontal scales, is transferred in a cascading manner toward shorter vertical and longer horizontal scales. Such a transfer results in the formation of strongly anisotropic inhomogeneities of wind velocity and temperature fields whose Eulerian spatial spectra (3D, vertical and horizontal) take the forms at high wavenumbers independent of the spectrum of the random sources themselves.

The spectrum formation model was verified on the results of airborne measurements of wind velocity fluctuations, temperature, and greenhouse gas concentrations conducted in September 2022. When decreasing horizontal scales, the spectra of fluctuations of wind velocity, temperature, and greenhouse gas concentrations (NO, NO_2, NO_x, SO_2) obtained both at the troposphere heights of about 9.5 km and in the lower troposphere (heights of 900 and 2900 m) indicated the existence of a transition on some scale, found in the paper, to a steeper spectrum (compared to −5/3) with a slope close to −3. It is important to note that the aircraft measurements were conducted in the Arctic region where according to

radiosonde data the temperature stratification was mostly stable ($N^2 > 0$) at flight heights with a weak change over height, except thin layers with $N^2 < 0$ of about 100 m thick, which were likely convectively unstable and intermittent at different heights with stably stratified layers. The vertical wind shear did not exceed 2 m s^{-1} km^{-1} as followed from the wind velocity profiles. It is also important to note that the transition to a steep spectrum was observed by us for both wind velocity fluctuations and gas concentrations measured by different methods and with the corresponding accuracy of measurements.

The presence of a steep section in the horizontal spectrum of wind velocity fluctuations with a slope of −3 has not been taken into account in most of modern spectrum models, aimed mainly at explaining the −5/3 mesoscale spectrum obtained by Nastrom and Gage (1985). In contrast to the earlier works on aircraft measurements (Myrup 1969; Shur 1962; Lilly and Lester 1974; Vinnichenko et al. 1980), which took into account the effect of stratification on the spectra along individual flight segments, in the recent works, on the contrary, the aircraft measurements have been performed on long traces with a large number (thousands) of segments (Cho et al. 1999; Callies et al. 2014, 2016; Skamarock et al. 2014; Lindborg 2015), apparently passing through areas with different uncontrolled stratification, including areas of small-scale turbulence under neutral stratification, and areas with stable stratification. We assumed that averaging spectra with different slopes (from −5/3 to −3) over a large number of segments should result in an average spectrum with some intermediate slope lying between −5/3 and −3 at short scales (from 6 km to 400 m).

Our results rather confirm the results of earlier aircraft measurements in which a steep high wavenumber part of the spectrum with a slope close to −3 was detected in the stably stratified layers of the troposphere and lower stratosphere. We obtained the individual spectra under approximately the same conditions characterized by stable stratification of the troposphere, which is typical for the Arctic region both for flight heights more than 9.5 km, and for lower tropospheric heights of 900 and 2900 m. Despite the differences in the forms of the obtained individual spectra, they all showed the presence of a steep region of the spectrum (compared to the −5/3 spectrum) at small scales, less than 6 km, The presence of a steep region in the spectrum, unnoticed in many recent works on aircraft measurements, makes us recall again the existence of the buoyancy subrange in the stably stratified medium, which passes at decreasing scales to the inertial range of the Kolmogorov–Obukhov turbulence.

The fluctuation spectra along different inclined traces of the aircraft were also estimated. Our assumption that each inclined track crossed the random layered inhomogeneities of wind velocity, temperature, and gas concentration, which were statistically homogeneous and stationary during the flight along two sections of the track lying in the height ranges of 1–5 km and 5–9 km, allowed us to estimate the spectra of these inhomogeneities over their vertical scales. The average vertical spectrum of the horizontal velocity fluctuations obtained during the descents and ascents of the aircraft along different inclined routes decreased according to the −3 law for the vertical scales decreasing from 300 to 30 m. A similar behavior of the vertical spectra was observed for the first time for the NO concentration fluctuations, which indicates a significant influence of the advection of air particles induced by internal waves and vortical motions on the formation of these spectra.

Acknowledgments. This work was supported by the Grant 075-15-2021-934 in the form of a subsidy from Ministry of Science and Higher Education of Russia.

Data availability statement. The airborne measurement dataset on which this paper is based is too large to be publicly archived with available resources. Some data on meteorological parameters and gas constituents may be shared by the author of the paper Boris Belan (bbd@iao.ru) upon request.

REFERENCES

Antokhin, P. N., and Coauthors, 2012: Optik-É AN-30 aircraft laboratory for studies of the atmospheric composition. *J. Atmos. Oceanic Technol.*, **29**, 64–75, https://doi.org/10.1175/2011JTECHA1427.1.

Bacmeister, J. T., S. D. Eckermann, P. A. Newman, L. Lait, K. R. Chan, M. Loewenstein, M. H. Proffitt, and B. L. Gary, 1996: Stratospheric horizontal wavenumber spectra of winds, potential temperature, and atmospheric tracers observed by high-altitude aircraft. *J. Geophys. Res.*, **101**, 9441–9470, https://doi.org/10.1029/95JD03835.

Belan, B. D., and Coauthors, 2022: Integrated airborne investigation of the air composition over the Russian sector of the Arctic. *Atmos. Meas. Tech.*, **15**, 3941–3967, https://doi.org/10.5194/amt-15-3941-2022.

Callies, J., R. Ferrari, and O. Bühler, 2014: Transition from geostrophic turbulence to inertia–gravity waves in the atmospheric energy spectrum. *Proc. Natl. Acad. Sci. USA*, **111**, 17 033–17 038, https://doi.org/10.1073/pnas.1410772111.

——, O. Bühler, and R. Ferrari, 2016: The dynamics of mesoscale winds in the upper troposphere and lower stratosphere. *J. Atmos. Sci.*, **73**, 4853–4872, https://doi.org/10.1175/JAS-D-16-0108.1.

Cho, J. Y. N., and Coauthors, 1999: Horizontal wavenumber spectra of winds, temperature, and trace gases during the Pacific Exploratory Missions: 1. Climatology. *J. Geophys. Res.*, **104**, 5697–5716, https://doi.org/10.1029/98JD01825.

Chunchuzov, I. P., 1996: The spectrum of high-frequency internal waves in the atmospheric waveguide. *J. Atmos. Sci.*, **53**, 1798–1814, https://doi.org/10.1175/1520-0469(1996)053<1798:TSOHFI>2.0.CO;2.

——, 2001: On the role of nonlinearity in the formation of the spectrum of atmospheric gravity waves. *Izv. Atmos. Oceanic Phys.*, **37**, 466–469.

——, 2002: On the high-wavenumber form of the Eulerian internal wave spectrum in the atmosphere. *J. Atmos. Sci.*, **59**, 1753–1774, https://doi.org/10.1175/1520-0469(2002)059<1753:OTHWFO>2.0.CO;2.

——, 2009: On the nonlinear shaping mechanism for gravity wave spectrum in the atmosphere. *Ann. Geophys.*, **27**, 4105–4124, https://doi.org/10.5194/angeo-27-4105-2009.

——, 2018: Nonlinear formation of the three-dimensional spectrum of mesoscale wind velocity and temperature fluctuations

in stably stratified atmosphere. *J. Atmos. Sci.*, **75**, 3447–3467, https://doi.org/10.1175/JAS-D-17-0398.1.

——, and S. Kulichkov, 2020: *Infrasound Propagation in an Anisotropic Fluctuating Atmosphere*. Cambridge Scholar Publishing, 355 pp.

Craig, G. C., and T. Selz, 2018: Mesoscale dynamical regimes in the midlatitudes. *Geophys. Res. Lett.*, **45**, 410–417, https://doi.org/10.1002/2017GL076174.

Dewan, E., 1997: Saturated-cascade similitude theory of gravity wave spectra. *J. Geophys. Res.*, **102**, 29 799–29 817, https://doi.org/10.1029/97JD02151.

——, and R. E. Good, 1986: Saturation and the "universal" spectrum for vertical profiles of horizontal scalar winds in the atmosphere. *J. Geophys. Res.*, **91**, 2742–2748, https://doi.org/10.1029/JD091iD02p02742.

Dörnbrack, A., S. D. Eckermann, B. P. Williams, and J. Haggerty, 2022: Stratospheric gravity waves excited by a propagating Rossby wave train—A DEEPWAVE case study. *J. Atmos. Sci.*, **79**, 567–591, https://doi.org/10.1175/JAS-D-21-0057.1.

Eckermann, S. D., 1999: Isentropic advection by gravity waves: Quasi-universal M^{-3} vertical wavenumber spectra near the onset of instability. *Geophys. Res. Lett.*, **26**, 201–204, https://doi.org/10.1029/1998GL900283.

Fritts, D. C., and M. J. Alexander, 2003: Gravity wave dynamics and effects in the middle atmosphere. *Rev. Geophys.*, **41**, 1003, https://doi.org/10.1029/2001RG000106.

——, T. Tsuda, S. Kato, T. Sato, and S. Fukao, 1988: Observational evidence of a saturated gravity wave spectrum in the troposphere and lower stratosphere. *J. Atmos. Sci.*, **45**, 1741–1759, https://doi.org/10.1175/1520-0469(1988)045<1741:OEOASG>2.0.CO;2.

Gage, K. S., 1979: Evidence for a $k^{-5/3}$ law inertial range in mesoscale two-dimensional turbulence. *J. Atmos. Sci.*, **36**, 1950–1954, https://doi.org/10.1175/1520-0469(1979)036<1950:EFALIR>2.0.CO;2.

Gisina, F. A., 1969: Spectral characteristics of turbulence in thermally stratified atmosphere. *Izv. Atmos. Oceanic Phys.*, **5**, 137–141.

Golitsyn, G. S., 2012: *Statistics and Dynamics of Natural Processes and Phenomena: Methods, Tools, Results* (in Russian). Krasand, 400 pp.

Gurvich, A. S., and I. P. Chunchuzov, 2008: Three-dimensional spectrum of temperature fluctuations in stably stratified atmosphere. *Ann. Geophys.*, **26**, 2037–2042, https://doi.org/10.5194/angeo-26-2037-2008.

——, and V. P. Kukharets, 2008: Horizontal and oblique spectra of temperature fluctuations in a stably stratified troposphere. *Izv. Atmos. Oceanic Phys.*, **44**, 717–722, https://doi.org/10.1134/S0001433808060042.

Hertzog, A., F. Vial, C. R. Mechoso, C. Basdevant, and P. Cocquerez, 2002: Quasi-Lagrangian measurements in the lower stratosphere reveal an energy peak associated with near-inertial waves. *Geophys. Res. Lett.*, **29**, 1229, https://doi.org/10.1029/2001GL014083.

Hines, C. O., 2001: Theory of the Eulerian tail in the spectra of atmospheric and oceanic internal gravity waves. *J. Fluid Mech.*, **448**, 289–313, https://doi.org/10.1017/S0022112001005973.

Imazio, P. R., P. D. Mininni, A. Godoy, N. Rivaben, and A. Dörnbrack, 2023: Not all clear air turbulence is Kolmogorov—The fine-scale nature of atmospheric turbulence. *J. Geophys. Res. Atmos.*, **128**, e2022JD037491, https://doi.org/10.1029/2022JD037491.

Kan, V., V. F. Sofieva, and F. Dalaudier, 2014: Variable anisotropy of small-scale stratospheric irregularities retrieved from stellar scintillation measurements by GOMOS/Envisat. *Atmos. Meas. Tech.*, **7**, 1861–1872, https://doi.org/10.5194/amt-7-1861-2014.

Lane, T. P., 2015: Gravity waves: Convectively generated gravity waves. *Encyclopedia of Atmospheric Sciences*, 2nd ed. G. R. North, J. Pyle, and F. Zhang, Eds., Academic Press, 171–179.

Li, Q., and E. Lindborg, 2018: Weakly or strongly nonlinear mesoscale dynamics close to the tropopause? *J. Atmos. Sci.*, **75**, 1215–1229, https://doi.org/10.1175/JAS-D-17-0063.1.

Lilly, D. K., and P. F. Lester, 1974: Waves and turbulence in the stratosphere. *J. Atmos. Sci.*, **31**, 800–812, https://doi.org/10.1175/1520-0469(1974)031<0800:WATITS>2.0.CO;2.

Lindborg, E., 1999: Can the atmospheric kinetic energy spectrum be explained by two-dimensional turbulence? *J. Fluid Mech.*, **388**, 259–288, https://doi.org/10.1017/S0022112099004851.

——, 2006: The energy cascade in a strongly stratified fluid. *J. Fluid Mech.*, **550**, 207–242, https://doi.org/10.1017/S0022112005008128.

——, 2015: A Helmholtz decomposition of structure functions and spectra calculated from aircraft data. *J. Fluid Mech.*, **762**, R4, https://doi.org/10.1017/jfm.2014.685.

Lumley, J. L., 1964: The spectrum of nearly inertial turbulence in a stably stratified fluid. *J. Atmos. Sci.*, **21**, 99–102, https://doi.org/10.1175/1520-0469(1964)021<0099:TSONIT>2.0.CO;2.

——, and H. A. Panofsky, 1964: *The Structure of Atmospheric Turbulence*. John Wiley and Sons, 244 pp.

Monin, A. S., and A. M. Yaglom, 1975: *Statistical Fluid Mechanics: Mechanics of Turbulence*. Vol. 1. MIT Press, 769 pp.

Myrup, L. O., 1969: Turbulence spectra in stable and convective layers in the free atmosphere. *Tellus*, **21A**, 341–354, https://doi.org/10.3402/tellusa.v21i3.10089.

Nappo, C. J., 2012: *An Introduction to Atmospheric Gravity Waves*. International Geophysics Series, Vol. 102, Academic Press, 321 pp.

Nastrom, G. D., and K. S. Gage, 1985: A climatology of atmospheric wavenumber spectra of wind and temperature observed by commercial aircraft. *J. Atmos. Sci.*, **42**, 950–960, https://doi.org/10.1175/1520-0469(1985)042<0950:ACOAWS>2.0.CO;2.

——, D. C. Fritts, and K. S. Gage, 1987: An investigation of terrain effects on the mesoscale spectrum of atmospheric motions. *J. Atmos. Sci.*, **44**, 3087–3096, https://doi.org/10.1175/1520-0469(1987)044<3087:AIOTEO>2.0.CO;2.

Phillips, O. M., 1967: Theoretical and experimental study of gravity wave interactions. *Proc. Roy. Soc. London*, **299A**, 104–119, https://doi.org/10.1098/rspa.1967.0125.

Poblet, F. L., J. L. Chau, J. F. Conte, V. Avsarkisov, J. Vierinen, and H. C. Asokan, 2022: Horizontal wavenumber spectra of vertical vorticity and horizontal divergence of mesoscale dynamics in the mesosphere and lower thermosphere using multistatic specular meteor radar observations. *Earth Space Sci.*, **9**, e2021EA002201, https://doi.org/10.1029/2021EA002201.

Schumann, U., 2019: The horizontal spectrum of vertical velocities near the tropopause from global to gravity wave scales. *J. Atmos. Sci.*, **76**, 3847–3862, https://doi.org/10.1175/JAS-D-19-0160.1.

Selz, T., L. Bierdel, and G. C. Craig, 2019: Estimation of the variability of mesoscale energy spectra with three years of COSMO-DE analyses. *J. Atmos. Sci.*, **76**, 627–637, https://doi.org/10.1175/JAS-D-18-0155.1.

Shur, G. N., 1962: Experimental investigations of the energy spectrum of atmospheric turbulence. *Tr. Tsentr. Aerol. Obs.*, **43**, 79–90.

Skamarock, W. C., S.-H. Park, J. B. Klemp, and C. Snyder, 2014: Atmospheric kinetic energy spectra from global high-resolution nonhydrostatic simulations. *J. Atmos. Sci.*, **71**, 4369–4381, https://doi.org/10.1175/JAS-D-14-0114.1.

Stephens, B. B., E. J. Morgan, J. D. Bent, R. F. Keeling, A. S. Watt, S. R. Shertz, and B. C. Daube, 2021: Airborne measurements of oxygen concentration from the surface to the lower stratosphere and pole to pole. *Atmos. Meas. Tech.*, **14**, 2543–2574, https://doi.org/10.5194/amt-14-2543-2021.

Vinnichenko, N. K., N. Z. Pinus, S. M. Shmeter, and G. N. Shur, 1980: *Turbulence in the Free Atmosphere*. 2nd ed. Springer, 310 pp.

Waite, M. L., and C. Snyder, 2014: Comments on "Indications of stratified turbulence in a mechanistic GCM." *J. Atmos. Sci.*, **71**, 854–857, https://doi.org/10.1175/JAS-D-13-0176.1.

Yuan, W., J. Xu, Y. Wu, J. Bian, and H. Chen, 2009: Vertical wavenumber spectra of atmospheric ozone measured from ozonesonde observations. *Adv. Space Res.*, **43**, 1364–1371, https://doi.org/10.1016/j.asr.2009.01.008.

Žagar, N., D. Jelić, M. Blaauw, and P. Bechtold, 2017: Energy spectra and inertia–gravity waves in global analyses. *J. Atmos. Sci.*, **74**, 2447–2466, https://doi.org/10.1175/JAS-D-16-0341.1.

Zhang, F., J. Wei, M. Zhang, K. P. Bowman, L. L. Pan, E. Atlas, and S. C. Wofsy, 2015: Aircraft measurements of gravity waves in the upper troposphere and lower stratosphere during the START08 field experiment. *Atmos. Chem. Phys.*, **15**, 7667–7684, https://doi.org/10.5194/acp-15-7667-2015.